HNOTE 878

Efficiency of the eTRD in SELEX

Jorge Amaro Reyes, Jürgen Engelfried
Instituto de Física,
Universidad Autónoma de San Luis Potosí, México

January 2006

Abstract

The efficiency of the eTRD for the identification of positrons (electrons) is measured using data from SELEX. The Electromagnetic Calorimeter (PHOT2) is used to obtain a sample of e^+ (e^-) via E/p. We also studied the miss-identification of pions using a sample of $\bar{\Lambda}^0$ (Λ^0). We studied different cuts for the identification of positrons (electrons). All measurements are performed as a function of momentum.

For a study of the semileptonic decay $\Lambda_c^+ \rightarrow \Lambda(1520)e^+\nu$ we have to know the efficiency for identifying positrons in the eTRD. Details of the semileptonic analysis can be found in H879 [1].

This note is a translation (Spanish original) from the relevant chapter in the PhD thesis of Jorge Amaro.

Contents

1 Method

The efficiency for detecting or identifying is the probability of detecting or identifying an event if it really took place.

The identification efficiency depends on the variables which describe the event, as well as on the physical mechanism on which the identification process is based. If redundant information within an experiment is available, the identification efficiency of a complex detector can be evaluated with real data from the experiment. To measure the efficiency, we need an event sample for which its identification is independent of the detector in question. If our detector responds in n out of N events within our identification criteria,

$$\varepsilon = \frac{n}{N} \tag{1}$$

is an estimator for the efficiency.

To measure the efficiency of the eTRD for identifying positrons (electrons), using real data, requires the selection of a sample of the particles in question. We obtain the lepton sample with the help of the electromagnetic calorimeter, PHOT2. We identify the leptons using E/p, where E is the energy deposited in the calorimeter, and p is the momentum of the charged track measured by the magnetic spectrometer(s). Positrons (electrons) deposit all their energy in the calorimeter, while hadrons deposit only a fraction of their energy, and muons only deposit very little energy corresponding to minimum ionization.

After we obtained our sample of positrons (electrons) with the help of PHOT2, we analyze the response of the eTRD to these particles with two methods: *cluster-counting* and *likelihoods*, both based mainly in the number of transition radiation photons emitted and detected. The number of photons emitted is proportional to γ, positrons and electrons emit more photons than hadrons at the same momentum.

The efficiency of the eTRD for the identification of positrons (electrons) depends on momentum p, and we determine $\varepsilon(p) = n(p)/N(p)$, where

> $N(p)$ is the number of particles called identified in PHOT2 for a given momentum(interval) p
>
> $n(p)$: number of particles identified as the same particle in the eTRD.

The particle identification in the eTRD by any of the before mentioned methods is performed by requiring some cut in the identification criteria. Some hadrons will pass the cut as well and will be wrongly identified as leptons. We have to compromise between the requirements of an as high as possible efficiency and as low as possible hadronic contamination of the identified leptons. From this follows that we not only have to determine the efficiency for identifying leptons, but also quantify the probability to wrongly identify a hadron as a lepton, or the *miss-identification probability*. In our case, the main source of particles which could be miss-identified as leptons are pions.

The pion sample is obtained by reconstructing $\Lambda^0 \to p\pi^-$ and $\bar{\Lambda}^0 \to \bar{p}\pi^+$. To measure the miss-identification, in this case $N(p)$ is the number of pions

from the Λ decays and $n(p)$ is the number of pions identified as leptons by the eTRD. Here $\varepsilon(e|\pi)$ denotes the probability to identify a π^+/π^- as a positron (electron).

2 The SELEX eTRD and PHOT2

SELEX has various particle identification systems. In this analysis we use the Transition Radiation Detector for the separation of electrons from hadrons (eTRD) and the lead-glass electromagnetic calorimeters, build to measure deposited energy of mainly γs and electrons, specially PHOT2. The eTRD and PHOT2 detectors are located within the spectrometer M2, between the spectrometer magnets M2 and M3, as shown in fig. 1.

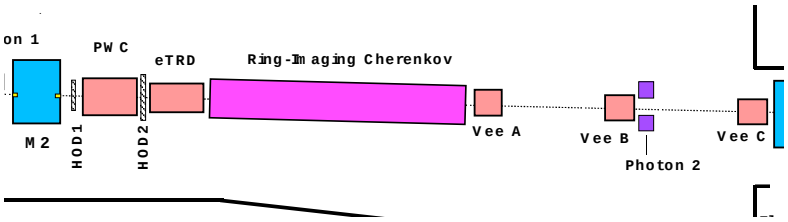

Figure 1: Schematic of the M2 spectrometer, for the location of the eTRD and PHOT2.

2.1 The SELEX Lead-glass Calorimeters

Three Electromagnetic Calorimeters are located at the end of each of the spectrometers M1, M2, and M2. To allow the passage of higher energy particles to later stages of the experiment, each of them has a central hole, the first two matching the size of the hole of the following magnet, the last a smaller hole for just the beam. The lead glass has a density of $4.1\,\mathrm{g/cm^3}$ and a radiation length of 2.5 cm. The first two calorimeters consist of blocks of two different lateral sizes, $4.25 \times 4.25 \times 34\,\mathrm{cm^3}$ for the central part, and $8.5 \times 8.5 \times 34\,\mathrm{cm^3}$ for the outer parts, respectively [3]. The third calorimeter is constructed from same-size blocks [4].

2.2 The SELEX eTRD

The SELEX Electron Transition Radiation Detector (eTRD) is divided into six modules within the M2 spectrometer. In each module, the transition radiation is generated by 200 17 μm polypropylene sheets. A MWPC of $103 \times 63\,\mathrm{cm^2}$ with a wire spacing of 4 mm, filled with a mixture of Xe and methane as counting gas, detects the radiation [2]. Electrons have a much higher γ as pion (or other heavier particles) of the same energy, and, consequently, produce more

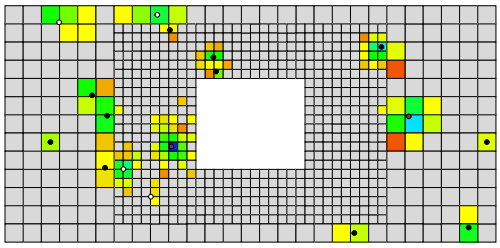

Figure 2: Beam-view of PHOT2. The colored blocks show the deposited energy in this reconstructed event. The black points correspond to the reconstructed position of a photon cluster, and the white points for other neutral particles. Colored points depict the position where a charged particle hit the detector.

TR photons, which lead to a higher number of detected "clusters" in the TRD chambers.

3 Software Implementation of the Method

For the measurement of the identification efficiency for positrons (electrons) we require that candidate tracks fulfill the following conditions:

coming from the vertex region

have a m1 and m2 segment

are identified as positrons (electrons) in PHOT2

fall within the geometrical acceptance of the eTRD

The most important are the criteria used to identify the particles in the calorimeter and the eTRD. The standard SELEX analysis code in *soap* has identification code implemented for both detectors.

3.1 Particle Identification in the Calorimeters

The particles which reach the calorimeter produce an electromagnetic shower and, due to the segmentation of the detector, the energy is deposited in various blocks. The group of blocks is called "cluster". The reconstruction algorithm for charged particles starts with locating a cluster and the deposited energy. After this, the impact point and the particle type are reconstructed.

For charged particle identification, tracks measured in the magnetic spectrometers are extrapolated to the calorimeter and their impact point is determined. For each cluster the impact point is compared with the cluster center within pre-established limits. Once accepted, the particle type is assigned depending in a χ^2_{pht} of the energy, reconstructed momentum and cluster (shower)

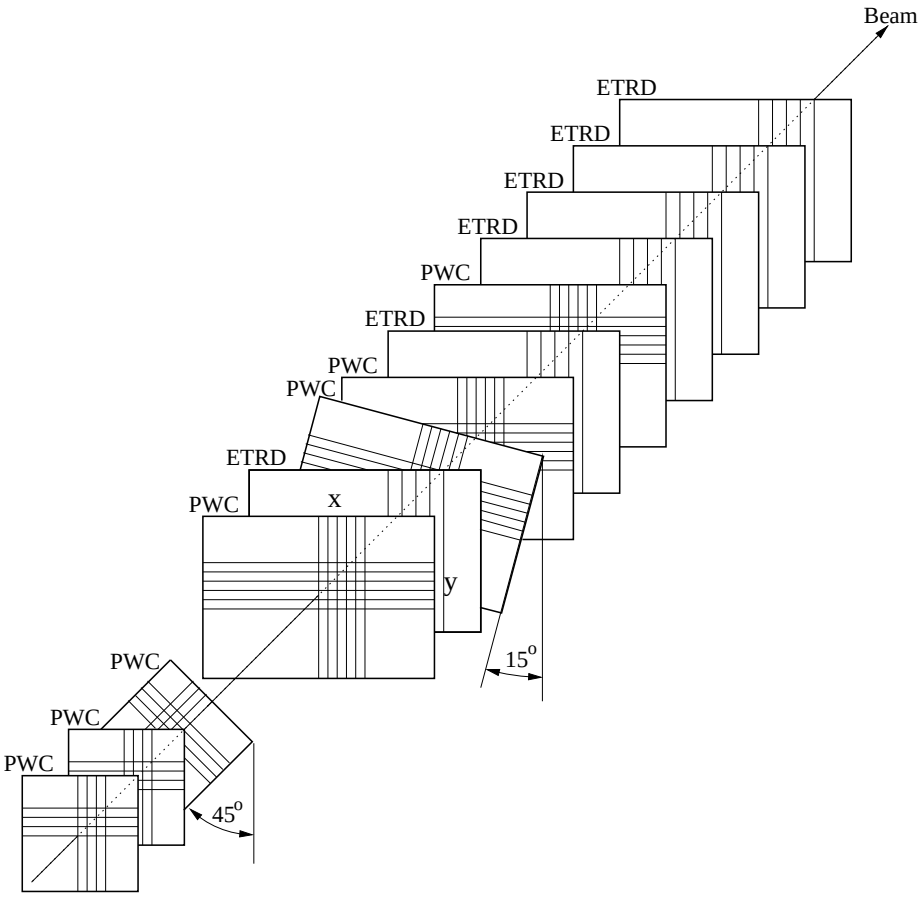

Figure 3: Schematic of the eTRD and tracking chambers in M2.

id_adcgam	Identified Particle
1	Photon
2	Electron (positron)
4	Neutral hadron
5	Muon
8	Charged hadron

Table 1: Particle identification code of the photon software; `id_adcgam(1,igam)` contains the type of the identified particle.

shape [5]. For the positron (electron) identification it is important to note that for the E/p value the pre-defined cut in *soap* is: $\delta_{phot} = 0.25$. We will see later

that is is not sufficient for the determination of the eTRD efficiency.

We implemented the method via the user routine in *soap*, *user.F*. It is based in part on *etr_phot.F*, the routine which identifies "tracks" with the help of PHOT2. The particle identification with the calorimeters is performed in the routine *trkmatch_pht.F*, which fills information into `id_adcgam(1,igam)`; the codes associated with each identified particle are shown in table 1.

3.2 Particle Identification in the eTRD

Charged Particles passing the eTRD produce Transition Radiation. In the wire chambers, these x-ray photons generate ionization "clusters", which are detected and counted along the trajectory of the particles in the different eTRD modules.

For the particle identification in the eTRD two methods are employed:

- *Likelihood* Method.
- *Cluster-Counting* Method.

The likelihood method finds for a given track the probabilities that the clusters detected along the trajectory have been produced by e, π, K or p, with a certain Lorentz-factor γ. γ is obtained assuming the mass of the different particle hypotheses, knowing the momentum of the trajectory. In the following, $\mathcal{L}(e)$ denotes the likelihood that the track under analysis is a positron (electron), $\mathcal{L}(\pi)$ that it is a pion and $\mathcal{L}(p)$ that it is a proton.

The cluster-counting method is simply summing up the number of clusters detected for a given trajectory; in this case it is not necessary to know the momentum of the track.

Both algorithm are implemented within *soap* in the routine *etr_driver.F* and its subroutines. The routine *etr_likeli.F* obtains the likelihoods for each track and fills the information into the variables: `prb(j,i)`, `lkhr1_etr` and `lkhr2_etr`; in table 2 we show more detailed information. The total number of clusters is accessible in `sumcl_etr(i)`.

Variable names	"Likelihood"
`prb(1,i)`	$\mathcal{L}(e)$
`prb(2,i)`	$\mathcal{L}(\pi)$
`prb(3,i)`	$\mathcal{L}(p)$
`lkhr1_etr`	$\mathrm{Log}_{10}(\mathcal{L}(e)/\mathcal{L}(\pi))$
`lkhr2_etr`	$\mathcal{L}(e)/(\mathcal{L}(e)+\mathcal{L}(\pi))$

Table 2: Variables in the analysis code which contain the likelihoods determined for different particle hypothesis for every track. $\mathcal{L}(e)$, $\mathcal{L}(\pi)$ and $\mathcal{L}(p)$ denote the likelihoods that the track in question is a positron, pion, or a proton, respectively.

Positrons (electrons) emit more transition radiation photons than pions; for this reason a cut in N_{Cl} is an adequate criteria to separate positrons from

pions. The likelihood method the identification criterion used here is the logarithm of the ratio of the likelihoods for being an electron to being a pion: $Log_{10}(\mathcal{L}(e)/\mathcal{L}(\pi))$. To facilitate the writing we define:

$$\mathcal{L}(e/\pi) \equiv Log_{10}(\mathcal{L}(e)/\mathcal{L}(\pi)). \tag{2}$$

4 Control Histograms for PHOT2

It is necessary to know the response of PHOT2 to particles depositing energy in it. The figures 4 and 5 show the distribution of E/p of charged particles reaching PHOT2. For this figure we selected some data where the eTRD already selected some electron to get some feeling on the response of calorimeter.

Positrons (electrons), which deposit their total energy into the calorimeter, form a peak centers around 1.0 en the E/p distribution shown in figure 4. To take into account the width of the peak, we use a parameter (δ_{phot}) which determines the acceptance window within we consider a particles as lepton; in other words, for a particle to be identified as a positron or electron we require

$$1 - \delta_{phot} < E/p < 1 + \delta_{phot}. \tag{3}$$

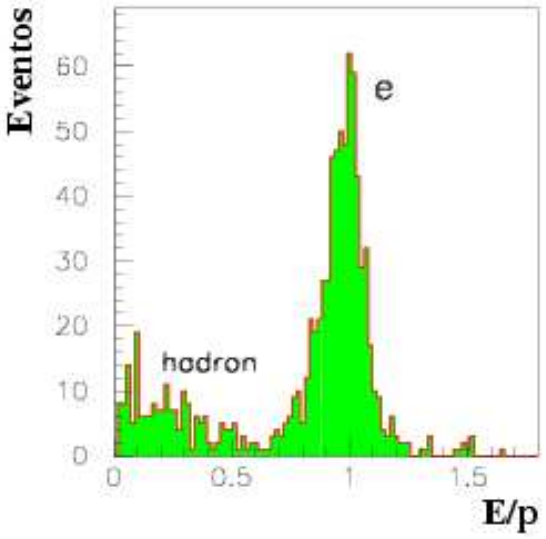

Figure 4: E/p distribution for positrons (electrons) reaching PHOT2.

The E/p distribution for pions reaching PHOT2 is shown in figure 5. Pions only deposit a fraction of their energy in the calorimeter, and present values smaller than 1.0 in the E/p distribution.

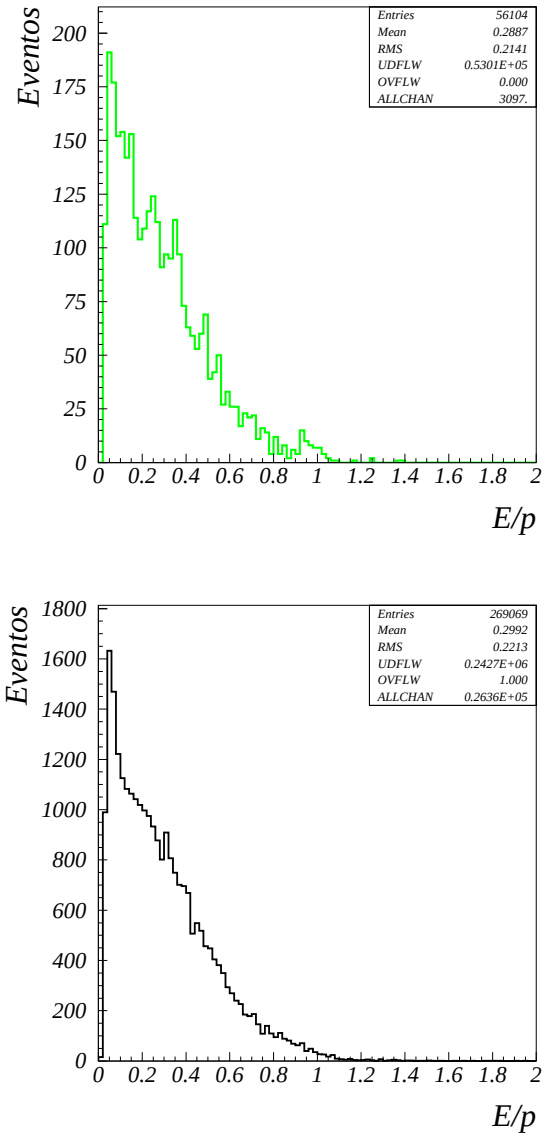

Figure 5: E/p distributions for pions reaching PHOT2. Top π^+. Bottom: π^-. The pions are select from $\Lambda^0 \to p\pi^-$ and $\bar{\Lambda}^0 \to \bar{p}\pi^+$ decays.

5 The eTRD Efficiency

The sample of positrons (electrons) needed to measure the efficiency of the eTRD for identifying positrons, $\varepsilon(e^+)$, and electrons, $\varepsilon(e^-)$, is obtained using PHOT2. The data sample used in this study are the *out4* outputs from pass1 processing (containing "strange" reconstructions). These data files were readily available in San Luis Potosí. Using the groups *pb, pc, pd, pe, pf, pg, ph, px, py, pz,* and *pp* allowed us also to study the response of the eTRD as a function of time (See section 7.1 and appendix F.

5.1 The lepton sample

The E/p distribution for particles reaching PHOT2 is shown in figure 6. Positrons (electrons) present a peak around 1.0 in this distribution, but there a large number of entries with E/p values smaller than 1.0 related to charged hadrons. The entries in the region around 1.0 determine our lepton sample. But we also

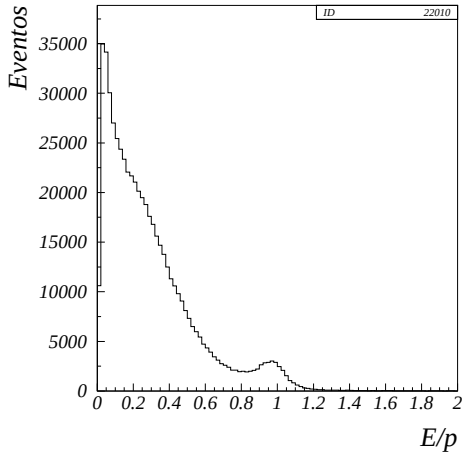

Figure 6: E/p distribution for charged (both charges) particles reaching PHOT2. The associated tracks have segments in vx, m1, and m2, and are within the geometrical acceptance of the eTRD.

observe a possible background from hadrons contaminating our lepton sample. Just selecting with a cut around 1.0 in E/p is not adequate, since the hadronic contamination would lead to an underestimation of the efficiency.

To emphasis the point some more, we adjust the sum of a Gaussian corresponding to the lepton signal and an exponential corresponding to the hadronic

component to the distribution. The fit function is:

$$\mathcal{F} = be^{-bx} + \frac{1}{\sqrt{2\pi}\sigma} e^{-\frac{(x-<x>)^2}{2\sigma^2}} \tag{4}$$

Figure 7 shows the results of the fit with equation 4 (black line) to the data shown in figure 6. Plotting the Gaussian and the exponential independently, we can appreciate how the hadronic component (blue line) contaminates the leptonic signal (red line). We see that a simple selection with a cut $1 \pm \delta_{phot}$, for example $\delta_{phot} = 0.25$, will result in a contaminated leptonic sample.

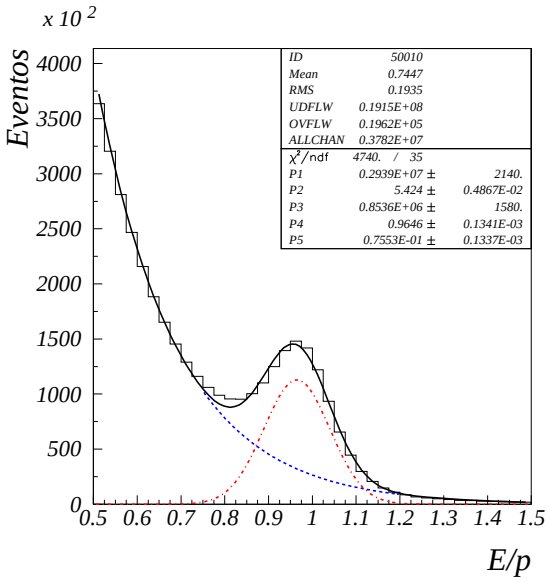

Figure 7: E/p distributions for particles reaching PHOT2. The black line represents the result of fitting the sum of a Gaussian and an exponential (representing the leptonic and hadronic component) to the distribution; the fit parameters are shown in the box (P1: Normalization of the exponential, P2: decay parameter of the exponential, P3, P4, P5: normalization, center, and sigma of the Gaussian). Gaussian (red) and exponential (blue) plotted independently.

To avoid (or better reduce) a possible hadronic contamination we use as additional criteria the identification algorithm described in section 3.1. Figure 8 shows the E/p distributions for leptons and hadrons identified in PHOT2. The blue histogram corresponds to hadrons and the magenta histogram to leptons, the continuous lines are the functions from fig. 7 with the same parameters. We can see that in some regions the fit and the selection criteria in the photon software coincide marvelously.

The leptonic distribution (magenta histogram) in fig. 8 contains a hadronic contamination between 0.72 and 0.92 as shown by the blue line. For this reason

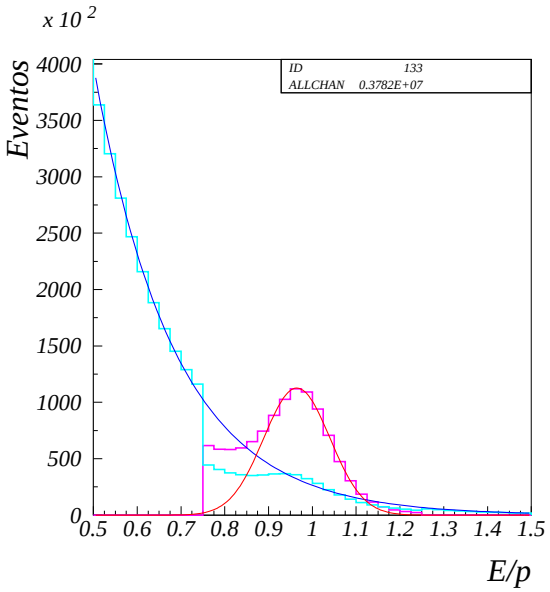

Figure 8: E/p distribution for particles reaching PHOT2, as determined with the additional identification algorithm described in section 3.1. Blue histograms: hadrons; magenta histogram: leptons. Blue and magenta line shows fit results from fig. 7.

we decided on a cut to have the cleanest possible leptonic sample within the E/p distribution of $1 \pm \delta_{phot}$ to be

$$\delta_{phot} = 0.05$$

The entries in the interval between 0.95 and 1.05 in the E/p distribution of fig. 8 (red histogram) is our sample of positrons (electrons) to measure the efficiency of the eTRD.

5.2 eTRD Response

The eTRD response is analyzed to determine the criteria to be applied to identify particles, especially to determine if a particle which passes the eTRD is a positron (electron) or a hadron.

Figure 9 shows the distribution of the number of cluster, N_{Cl}, and the ratio of Likelihoods $\mathcal{L}(e/hadron)$, for hadrons passing the eTRD. We observe that the number of clusters follow a Poisson distribution with a mean of about 1, while the likelihood distributions shows $\mathcal{L}(e/hadron) < 0$, meaning $\mathcal{L}(hadron) > \mathcal{L}(e)$.

Figure 10 shows the distribution of N_{Cl} and $\mathcal{L}(e/hadron)$ for leptons and hadrons passing the eTRD. Leptons generate a larger number of clusters along

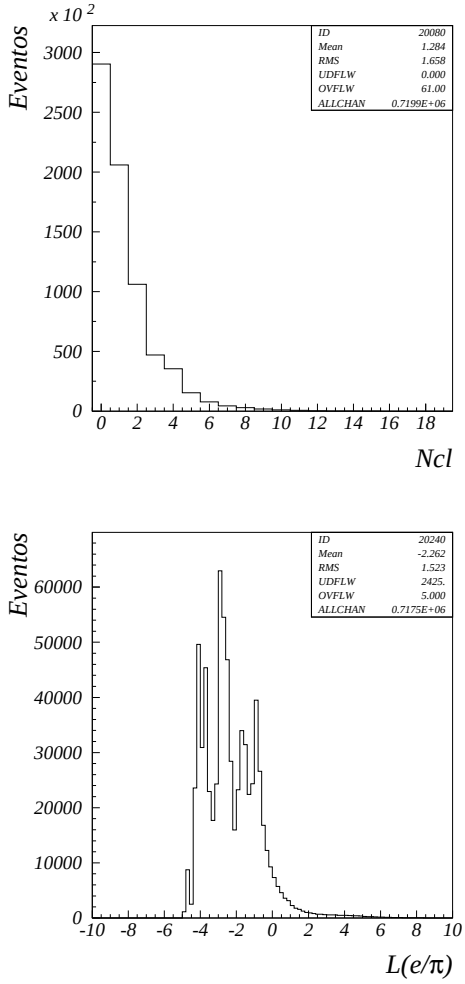

Figure 9: eTRD response to hadrons. top: N_{Cl}; bottom: $\mathcal{L}(e/\pi)$.

the trajectory as hadrons. Figure 10 (top) shows that the distribution of the number of clusters for leptons follows again a Poisson distribution with a mean value between 6 and 7. As opposed to the hadrons, leptons produce

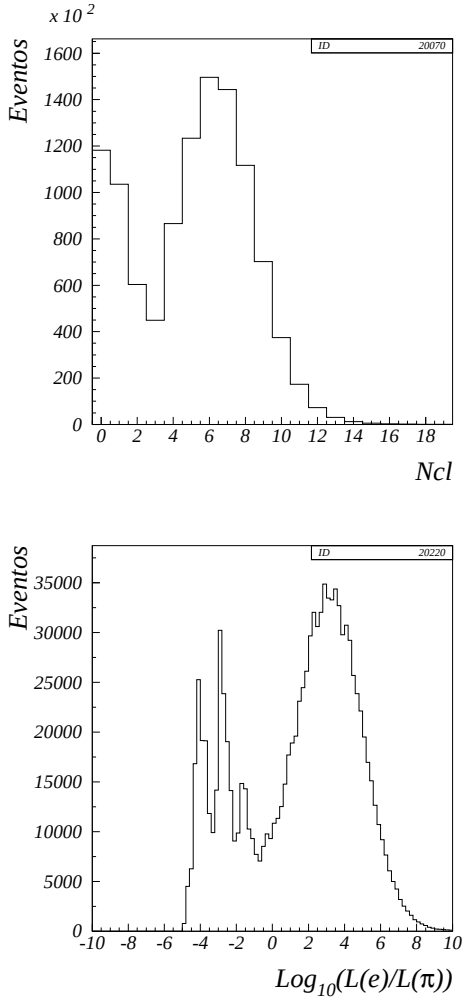

Figure 10: eTRD response to charged particles. Top: N_{Cl}; bottom: $\mathcal{L}(e/\pi)$.

$\mathcal{L}(e/hadron) > 0$ (see fig. 10 bottom) indicating that the lepton is more likely than a hadron, $\mathcal{L}(e) > \mathcal{L}(hadron)$.

5.2.1 Criteria for the identification of e^+/e^- with the eTRD

As mentioned before, the identification of positrons (electrons) with the eTRD can be performed by two methods: likelihoods and cluster counting.

Likelihood Method, $\mathcal{L}(\mathbf{e}/\pi)$. The condition for the identification of a positron (electron) is that the lepton interpretation is more likely than that of the pion interpretation, $\mathcal{L}(e) > \mathcal{L}(\pi)$. One adequate criterion would be:

$$\mathcal{L}(e/\pi) > 0, \tag{5}$$

in figures 11 and 30 (see appendix A) we observe clearly that leptons are found in this region.

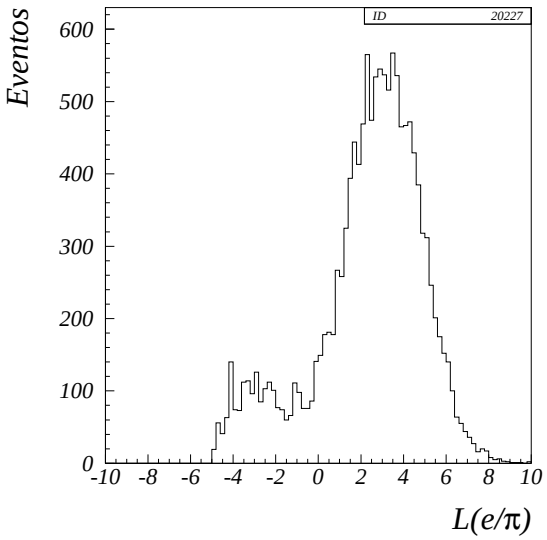

Figure 11: $\mathcal{L}(e/\pi)$ in the eTRD for leptons identified in PHOT2: el PHOT2: $id\_adcgam = 2$ and $\delta_{phot} = 0.05$.

Measuring the efficiency of the eTRD for the identification of positrons is necessary for the study of semileptonic decays in which these particles participate. We are particularly interested in studying the decay $\Lambda_c^+ \to \Lambda(1520)e^+\nu$. For this mode exist preselected data from pass1 and pass2 (recon-id 490), where the positron was identified by the eTRD with.

$$\mathcal{L}(e/\pi) > 0.5, \tag{6}$$

this is why we will determine later only for harder cuts the efficiency.
Cluster counting method, $\mathbf{N_{Cl}}$. Another criterion which allows to discriminate between positrons and electrons is the number of clusters detected while the particles passes the eTRD. We use

$$N_{Cl} > 3 \tag{7}$$

The number of clusters detected in the eTRD is shown in figures 12 and 31 (appendix B) and we see that the region with $N_{Cl} > 3$ corresponds to the clusters produced by positrons (electrons).

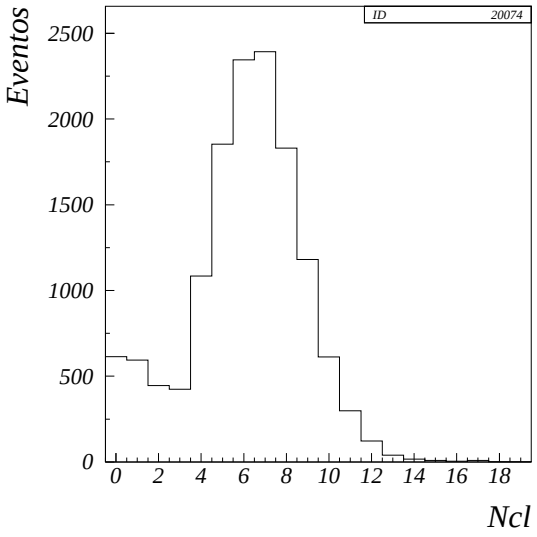

Figure 12: Number of Clusters in the eTRD for leptons identified in PHOT2, $\delta_{phot} = 0.05$.

After studying and understanding the response, we can now go on and perform the measurement of the efficiency of the eTRD. $\varepsilon(e)$, for the identification of positrons and electrons. As we will see later, the efficiency depend strongly on the criterion used to identify the positron (electron).

5.3 Efficiency of the eTRD – $\mathcal{L}(e/\pi)$

For the criterion of the likelihood ratio $\mathcal{L}(e/\pi)$, we obtain the efficiency of the eTRD for the identification of positrons, $\varepsilon(e^+)$, and electrons, $\varepsilon(e^-)$. The efficiency was obtained as a function of momenta.

Figure 13 shows the efficiencies for positrons (green triangles) and electrons (red circles).

Two comments have to be made about fig. 13. The first observation is that the efficiency decreases for momenta above $45\,\mathrm{GeV}/c$, and decrease abruptly above $\sim 120\,\mathrm{GeV}/c$. This is due to the hadronic contamination in the lepton sample, which increases with momenta, leading to an apparent decrease in eTRD efficiency. In appendix H, where we study the efficiency as a function of χ^2_{pht}, we demonstrate this argument.

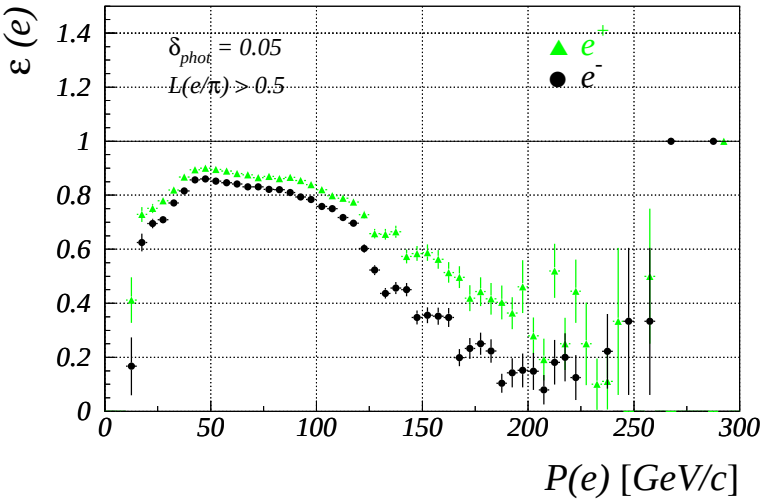

Figure 13: Efficiency of the eTRD for the identification of positrons electrons. $\mathcal{L}(e/\pi) > 0.5$ as identification criterion.

The second observation is related to the notable difference in the efficiency for identifying positrons and electrons, which is surprising, since the emission of transition radiation does not depend on the sign of the charge of the particle generating the radiation. We will defer the discussion to section 7.

In the appendix C, we show results from a systematic study for different $\mathcal{L}(e/\pi)$ and δ_{phot} cuts.

5.4 Efficiency of the eTRD – N_{Cl}

Using the number of clusters $N_{Cl} > 3$ detected from particle in the eTRD as criterion for identifying the positron (electron), we obtain fig. 14, where $\varepsilon(e^{\pm})$ is shown as a function of momentum.

Again we note a difference en the efficiency for electrons and positrons, as well as a decrease above 120 GeV/c, see also appendix H. In appendix D we show a systematic study for different cuts in N_{Cl} and δ_{phot}.

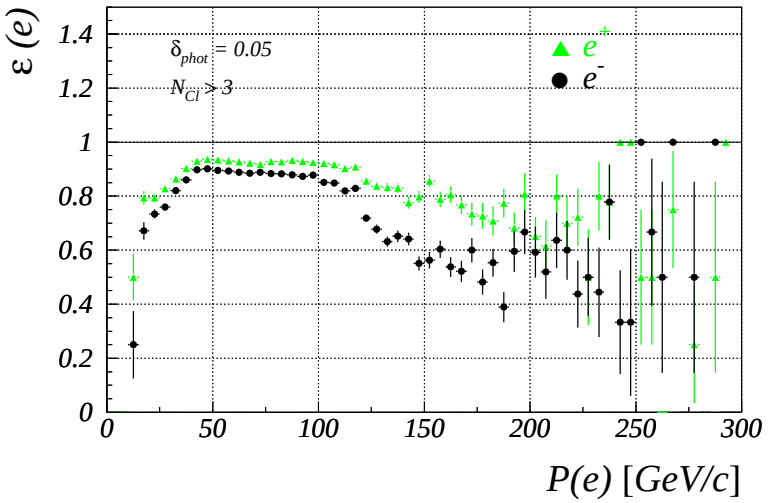

Figure 14: Efficiency of the eTRD for identifying positrons and electrons. $N_{Cl} > 3$ as identification criterion.

6 Miss-identification of pions

In parallel to determining the efficiency of the eTRD to identify leptons, we also have to know the probability that the eTRD identifies other particles as positrons (electrons).

We are mostly interested in separating pions from leptons, because they are the particles which most contribute to the false identification of positrons (electrons). To quantify this effect called miss-identification, we determine the probability that a real pion as identified as positron (electron), $\varepsilon(e|\pi)$.

6.1 Data sample: $\bar{\Lambda}^0$ and Λ^0

The data sample necessary is obtained reconstructing the decays $\Lambda \to p\pi^-$ and $\bar{\Lambda} \to \bar{p}\pi^+$. We used the data from a pass1 strip, *strip23*, readily available in San Luis Potosí. The distribution of invariant masses for Λ^0 and $\bar{\Lambda}^0$ are shown in figure 15.

6.2 The eTRD response to Pions

Here we study the eTRD response to pions which the detector. The distribution of $\mathcal{L}(e/\pi)$ for pions is shown in figure 16. Since the particles are pions, $\mathcal{L}(\pi) > \mathcal{L}(e)$, or $\mathcal{L}(e/\pi) < 0$, which coincides with what we see in the figure.

Pions generate fewer clusters along their trajectory than positron; see figures 9 and 10 where we show the distribution of the number of clusters detected for positrons (electrons) and hadrons respectively. The distribution of N_{Cl} detected for our pion sample is shown in figure 17, and is identical to the distribution for hadrons (figure 9(left)).

6.3 Pion Miss-identification – $\mathcal{L}(e/\pi)$

Here we will discuss the probability that a pion is identified as a positron (electron), $\varepsilon(e|\pi)$, using the likelihood method to identify the lepton.

Figure 18 shows the probability that a π^+/π^- is identifies as positron (electron). The distributions for both charges look similar, and even for momenta as high as $120\,\mathrm{GeV}/c$ the probability is below 2 % In rough numbers, only one out of 100 pions are identified as lepton by the eTRD.

6.4 Pion Miss-identification – N_{Cl}

Figure 19 shows the probability that a pion is identified as a lepton, using the cluster counting as identification criterion, We can see that on average ten out of 100 pions are considered to be leptons, about a factor 10 worse than in the case of the likelihood method.

We can define a rejection factor in the following way:

$$f_R(\pi) \equiv 1 - \varepsilon(e|\pi). \tag{8}$$

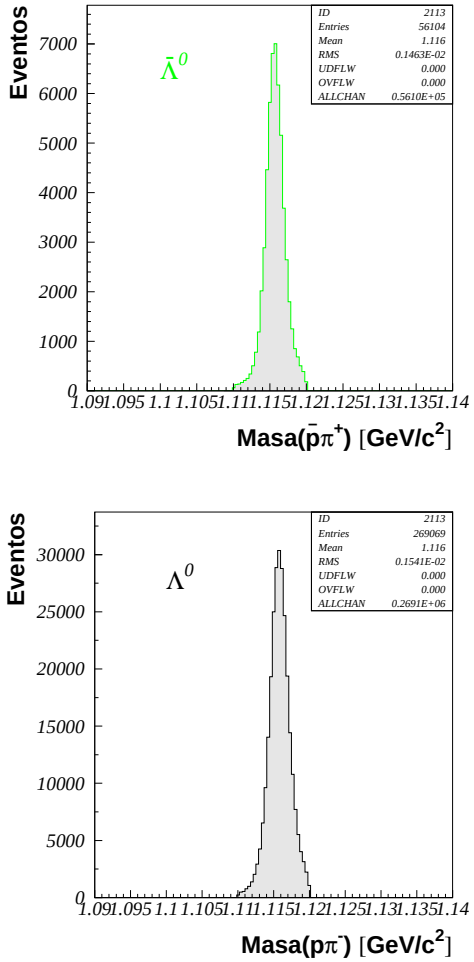

Figure 15: Invariant mass distribution for reconstructed $\bar{p}\pi^+$ (top), $p\pi^-$ (bottom) corresponding to $\bar{\Lambda}^0$ and Λ^0 respectively.

With this definition, $f_R(\pi^{\pm}) \sim 0.99$ for the likelihood method, and $f_R(\pi^{\pm}) \sim 0.90$ for the cluster counting method.

In appendix E, we present the results of study of miss-identification probabilities for pions for different cuts in $\mathcal{L}(e/\pi)$ and N_{Cl}.

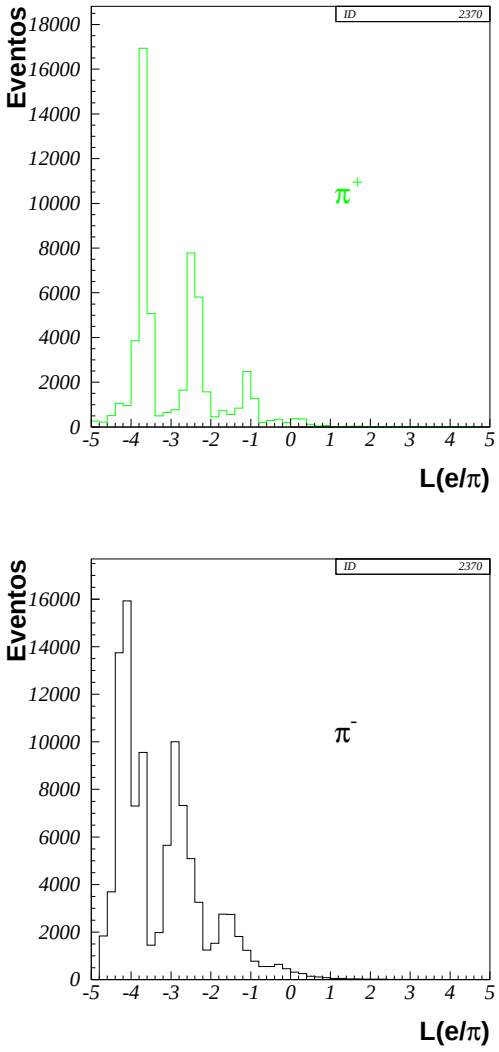

Figure 16: Distribution for $\mathcal{L}(e/\pi)$ for pions: top: π^+; bottom π^-.

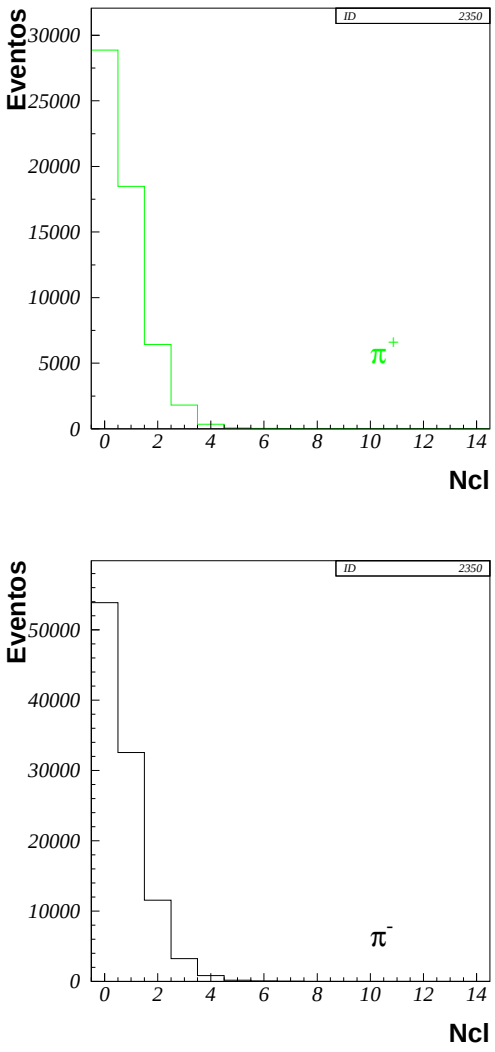

Figure 17: Distribution of the number of clusters N_{Cl} detected for pions passing the eTRD. top: π^+; bottom: π^-.

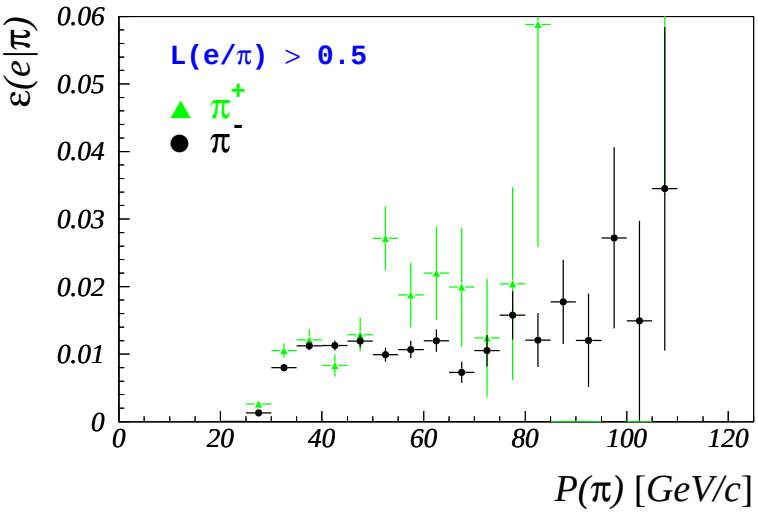

Figure 18: Miss-identification of pions. $\mathcal{L}(e/\pi) > 0.5$

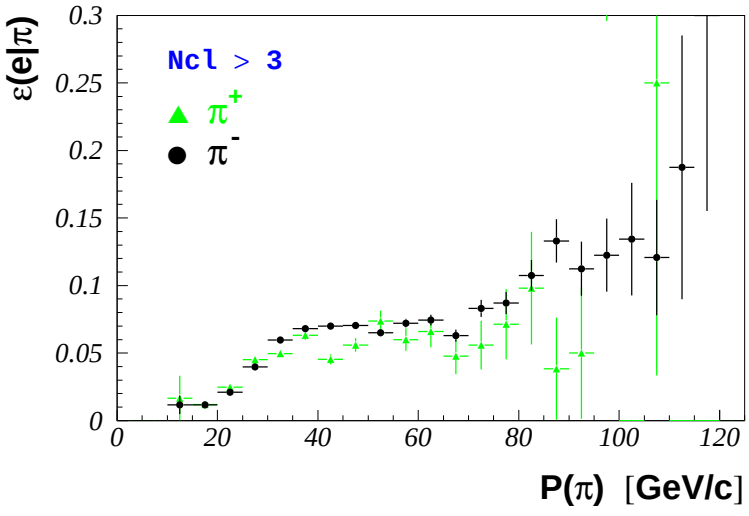

Figure 19: Miss-Identification of pions. $N_{Cl} > 3$.

7 Asymmetry in the eTRD Efficiency

The mechanism for the generation of transition radiation is independent on the sign of the charge of the particle producing the radiation. For this reason the efficiency of the eTRD to identify particles should be the same for electrons and positrons. But as we have seen before in fig. 13 and 14 there is a difference, which is present in both identification methods and for a variety of cuts, as shown in the figures in appendix C (figures 32, 33, 34) and D (figures 35, 36, 37).

A quantity which permits us to study this difference in efficiencies, the asymmetry $\mathcal{A}$, is defined as the ratio of efficiencies for the positron and the electron:

$$\mathcal{A} \equiv \frac{\varepsilon(e^+)}{\varepsilon(e^-)} \tag{9}$$

Figure 20 shows the asymmetry of the efficiency, $\mathcal{A}$, for different values of δ_{phot}. As δ_{phot} increases, the asymmetry increases as well; $\mathcal{A} > 1$, indicating that $\varepsilon(e^-) < \varepsilon(e^+)$.

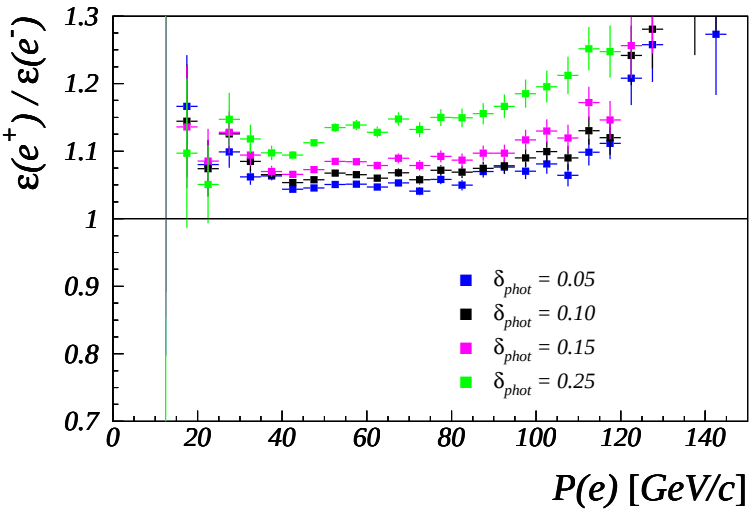

Figure 20: Asymmetry of the efficiency of the eTRD for identifying positron and electrons. Different cuts in δ_{phot} for the definition of the leptonic sample. $\mathcal{L}(e/\pi) > 0.5$.

As the efficiency is the ratio of the number of particles identified as leptons by the eTRD and the number of original leptons from the sample traversing the detector, we believe that the efficiency for electrons is underestimated, leading to the observed asymmetry. For some reason the eTRD "looses" electrons, or

the sample contains other particles than electrons. We investigated two possible reasons:

1 – *Ageing of the detector.*
It is possible that certain regions of the detector aged due to the particles passing thru the detector. Since most of the data were taken with negative beam, which could lead to a reduced efficiency in the regions corresponding to negative particles.

2 – *Hadronic contamination of the leptonic sample.*
The method used to define the leptonic sample includes the possibility of hadronic contamination of the sample. If the contamination for electrons is larger than for positrons, this could be an origin for the observed asymmetry.

7.1 eTRD Ageing

To analyze the eTRD response as a function of time, we determine the efficiencies for each of the groups *pb, pc, pd, pe, pf, pg, ph, px, py, pz* and *pp*, each of them corresponds to different time periods during the data taking, from January to September 1996.

Figure 21 shows the efficiencies of the eTRD for identifying positrons and electrons for each run group, and for different momentum ranges: $45-50\,\mathrm{GeV}/c$ (top of figure), $50-80\,\mathrm{GeV}/c$ (center), $80-85\,\mathrm{GeV}/c$ (bottom). The asymmetry in the first 3 groups *pb, pc, pd* is not as big as in the others (*pe, pf, pg, ph, px, py, pz, pp*), where it reaches about 4 %. The detector performance seems to be constant from group *pe* to group *pg* and from group *ph* to group *pz* for both particles, but $\varepsilon(e^+)$ is still larger than $\varepsilon(e^-)$. In the appendices F and G we show a more complete study of the asymmetries for different momenta and run groups.

The observed asymmetry could be caused by ageing in a part of the detector. The reduction in $\varepsilon(e^-)$, approximately 4 % less than $\varepsilon(e^+)$, can be due to effects for passing beam particles. The charged particles are bend by the magnetic fields. In SELEX, negatively charged particles are bend to the right, as seen in beam direction, while positive particles go in the other direction. Most of the time data taking was with negative beam ($600\,\mathrm{GeV}/c$), which gets deflected to the "negative" side, which can affect more the electron than the positron identification.

There is also a data set with positive beam (group *pp*). During this period all the magnetic fields were inverted, which means that all charged particles were also deflected to the other side. This gives us the opportunity to to study the results of this group, which offers us two possible outcomes: (1) it stays the same, or (2) the effect reverse.

If the efficiencies invert, this would mean direct evidence that the ageing effect on the right side (seen with the beam) is at least partly responsible for the observed asymmetry; if not, we have to look for another origin for our problem.

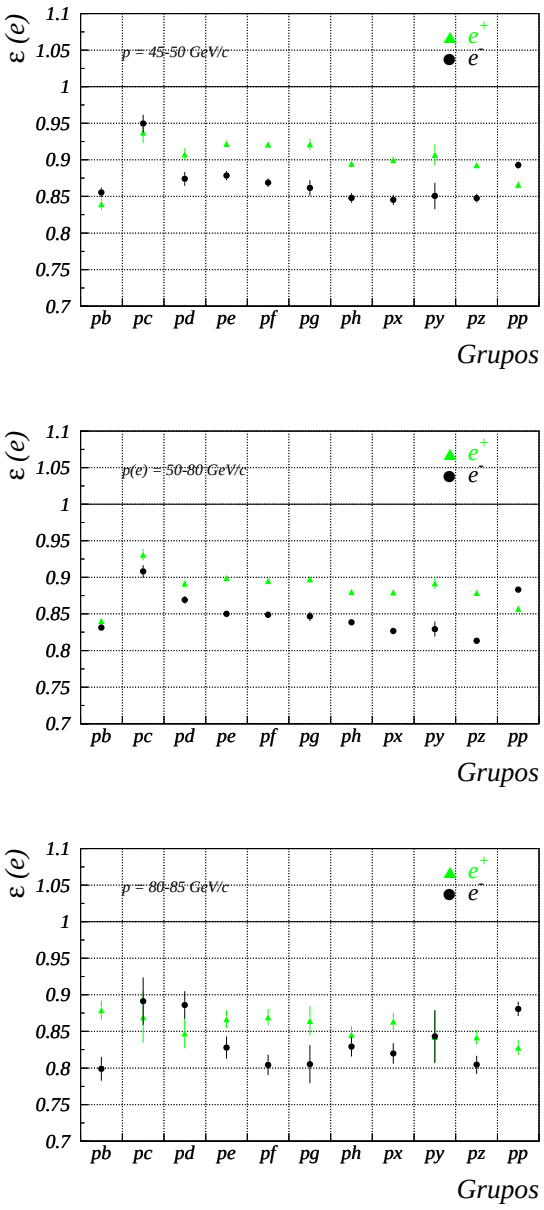

Figure 21: Efficiency of the eTRD for identifying positrons (green triangles) and electrons (black circles) for each run group and some momentum intervals. $\delta_{phot} = 0.05$, $\mathcal{L}(e/\pi) > 0.5$.

If we now look at the efficiencies of group *pp* shown in figure 21, we observe that the asymmetry inverses, $\varepsilon(e^+) < \varepsilon(e^-)$, as opposed to the other groups, $(\varepsilon(e^+) > \varepsilon(e^-))$. In addition the difference in efficiencies is nearly the same, only slightly smaller.

7.2 Hadronic Contamination in the leptonic sample

The asymmetry could be a consequence of the selection method for the leptonic sample. As we have seen before, the selection process has the possibility for a hadronic contamination of the sample. If the electron sample has a larger contamination than the positron sample, this could be the origin of the observed asymmetry if the efficiencies.

In figure 20 we can see that the asymmetry depends on the cut δ_{phot}, if its value increases the asymmetry increases as well.

This is understandable when we analyze separately the E/p distributions for positive and negative particles to determine the hadronic component, as in figures 22 and 23.

In the positron sample the contamination[1] is significant in the range for E/p from 0.75 to ~ 0.90, while in the electron sample the contamination is notable from 0.75 up to values of ~ 0.97, which leads to our conclusion that if we make whatever cut in δ_{phot} the electron sample has a higher hadronic contamination than the positron sample.

Selecting the sample with a cut of $\delta_{phot} = 0.05$, the hadronic contamination in the negative channel is relatively small (from 0.95 a 0.97) but larger than in the positive channel. We will now analyze in detail if this amount of contamination can generate the observed asymmetry.

To investigate deeper this argument, and to decide if the hadronic contamination is the cause of the asymmetry, we need a "cleaner" electron and positron sample, one where the contamination on both charges is negligible. We will try to use a harder cut in χ^2_{pht} of the cluster-shape for the deposited energy in the calorimeter.

Cleaner sample, $\chi^2_{pht} < 2$

Even with a harder cut in χ^2_{pht} for selecting the leptonic samples, the efficiency asymmetry stays about the same. The experimental points shown in figures 24 and 46 $(\chi^2_{pht} < 2)$[2] have the same behavior as the one shown in figure 21 $(\chi^2_{pht} < 20)$. For more detailed information please see appendix H, efficiency as function of χ^2_{pht}.

The decrease in the hadronic contamination increases both efficiencies: about 1 % for the positive channel and $\sim$ 2 % for the negative channel, and consequently the difference decreases from $\sim 5\%$ to $\sim 4\%$. Compare figures 24 and 21(center).

[1] Remember that the contamination is the difference between the dark blue line and the light blue histogram in the region of interest

[2] Some groups are missing because we lost some data due to a disk failure.

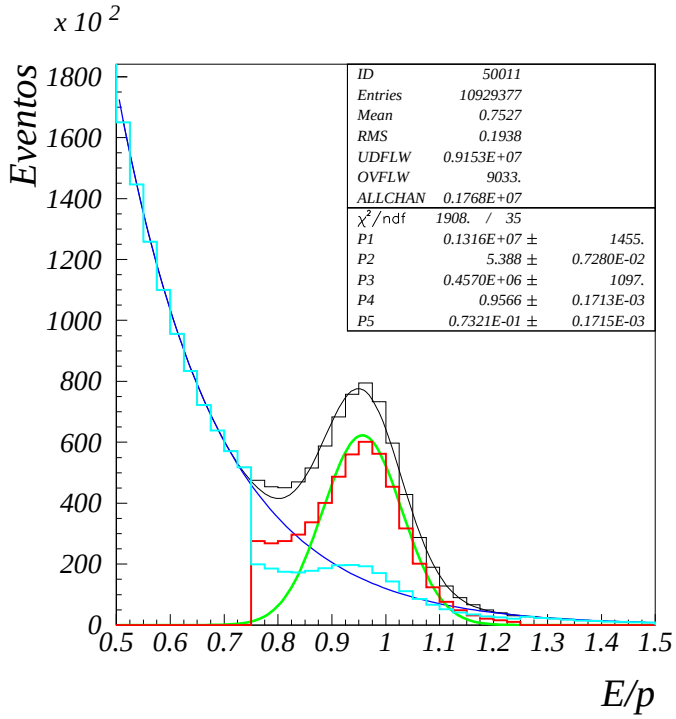

Figure 22: E/p distribution for positively charged particles reaching PHOT2. The continuous line represents the result of a fit of an exponential an a Gaussian; the parameters are shown in the box.

Figure 25 shows the average efficiency for the likelihood method (top) and cluster-counting (bottom). The graphs show a better behavior at momenta $> 120\,\mathrm{GeV}/c$. In appendix H we demonstrate that a harder cut in χ^2_{pht} reduces hadronic contamination at high momentum. For momenta below $45\,\mathrm{GeV}/c$ in general the efficiency decreases, but for some run groups (figures 40 and 41 en appendix F) the eTRD efficiency shows a constant behavior from about $25\,\mathrm{GeV}/c$.

Finally, the eTRD efficiency for the identification of positrons (electrons) is approximately 90 % as shown in figure 25.

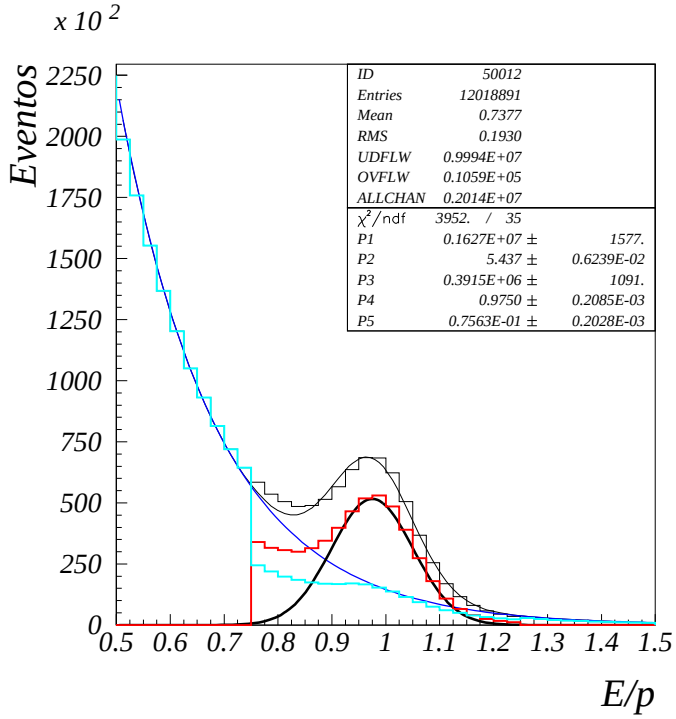

Figure 23: E/p distribution for negatively charged particles reaching PHOT2. The continuous line represents the result of a fit of an exponential an a Gaussian; the parameters are shown in the box.

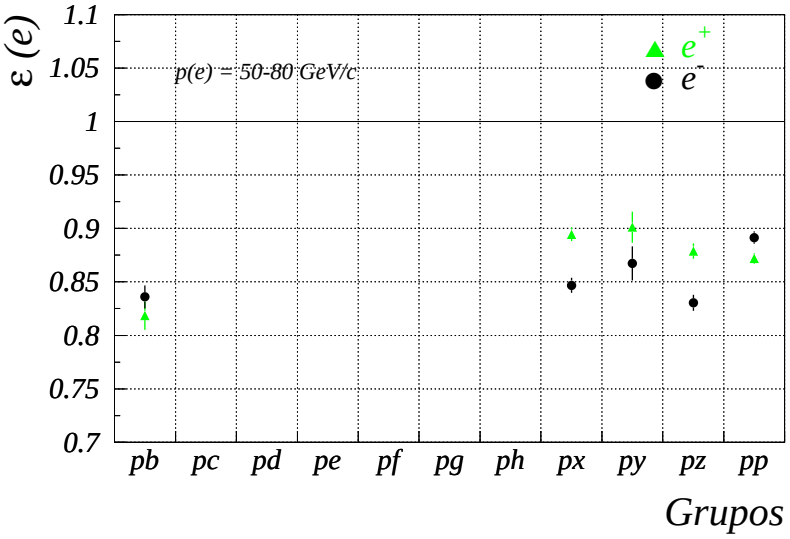

Figure 24: eTRD efficiencies for the identification for positrons (electrons), for different run groups. $\delta_{phot} = 0.05$, $\mathcal{L}(e/\pi) > 0.5$, $\chi^2_{pht} < 2$.

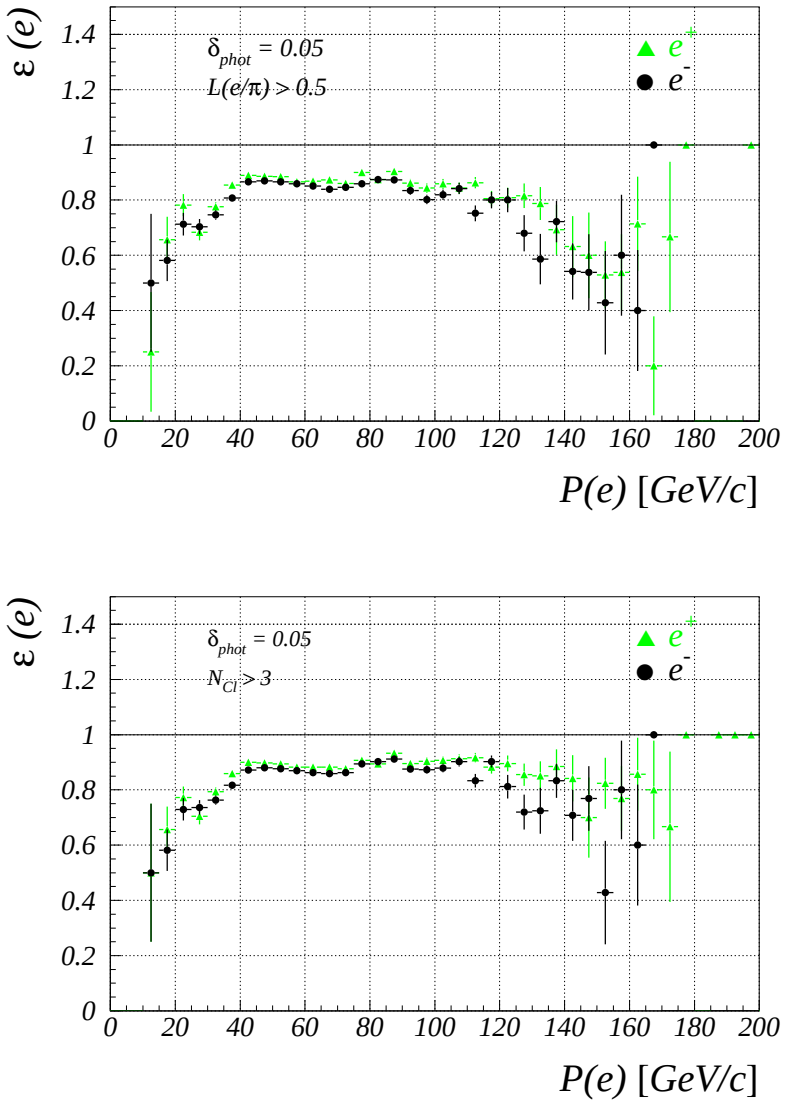

Figure 25: eTRD efficiency, $\chi^2_{pht} < 2$. top: likelihood method. bottom: cluster-counting.

8 Results

8.1 e^+/e^- efficiency vs $\pi^\pm$ rejection

There has to be a compromise between the eTRD efficiency for the identification of positrons (electrons) and the pion rejection, defined as $1 - \varepsilon(e|\pi)$. We show here $\varepsilon(e|\pi)$ vs $\varepsilon(e)$, and as parameters different cuts in $\mathcal{L}(e/\pi)$ and N_{Cl}, figures 26 and 27. As we make the cuts harder, $\varepsilon(e)$ decreases from 89 % to 60 % for $\mathcal{L}(e/\pi)$ and from 92 % to 55 % with N_{Cl}.

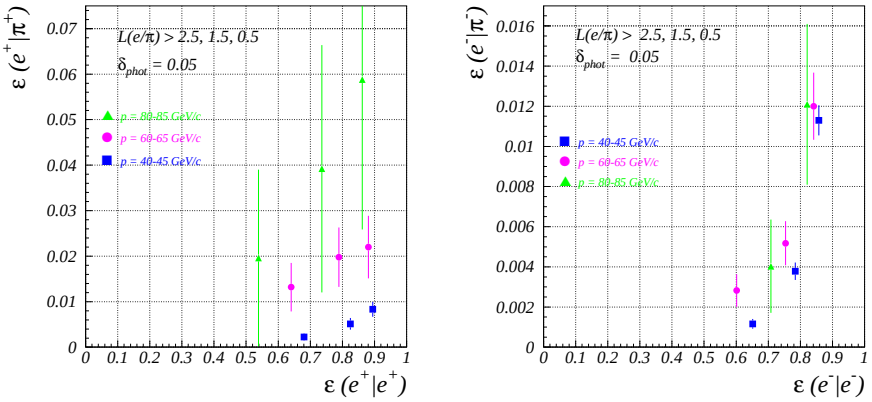

Figure 26: $\varepsilon(e|\pi)$ *vs* $\varepsilon(e)$, for values of $\mathcal{L}(e/\pi) > 0.5, 1.5, 2.5$. Left: positrons, right: electrons. $\delta_{phot} = 0.05$.

$P(e)$ $[GeV/c]$	$\mathcal{L}(e/\pi)$	$\epsilon(e^+)$	$\epsilon(e^+\|\pi^+)$	$\epsilon(e^-)$	$\epsilon(e^-\|\pi^-)$
40-45	0.5	0.89	0.008	0.85	0.011
	1.5	0.82	0.005	0.78	0.003
	2.5	0.68	0.002	0.65	0.001
60-65	0.5	0.88	0.021	0.84	0.012
	1.5	0.78	0.019	0.75	0.005
	2.5	0.64	0.013	0.60	0.002
80-85	0.5	0.86	0.058	0.82	0.012
	1.5	0.73	0.039	0.70	0.004
	2.5	0.53	0.019	0.53	0.0

Table 3: Efficiencies *vs* $\mathcal{L}(e/\pi)$. $\delta_{phot} = 0.05$. Values from fig. 26.

The pion rejection is higher with the likelihood method as with cluster-counting: 99 % and 90 %, respectively, for $\mathcal{L}(e/\pi) > 0.5$ and $N_{Cl} > 3$. These

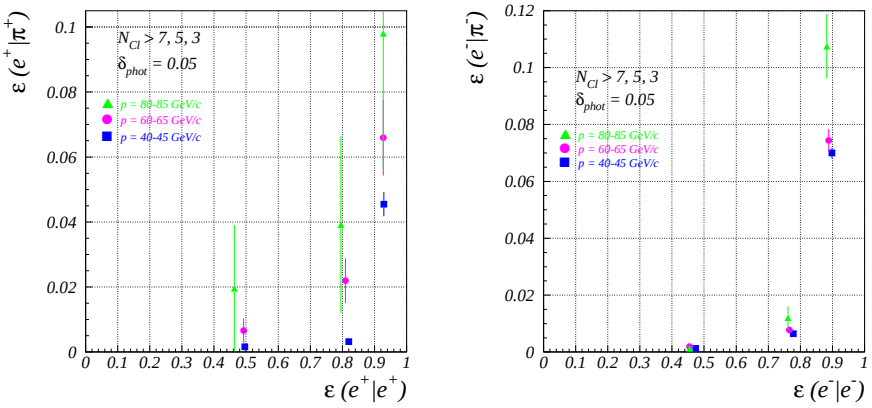

Figure 27: $\varepsilon(e|\pi)$ *vs* $\varepsilon(e)$. $N_{Cl} > 3, 5, 7$. Left: positrons;, right: electrons. $\delta_{phot} = 0.05$.

$P(e)$ $[GeV/c]$	N_{Cl}	$\epsilon(e^+)$	$\epsilon(e^+\|\pi^+)$	$\epsilon(e^-)$	$\epsilon(e^-\|\pi^-)$
40-45	3	0.929	0.045	0.898	0.069
	5	0.819	0.003	0.778	0.006
	7	0.495	0.001	0.473	0.001
60-65	3	0.927	0.065	0.888	0.074
	5	0.809	0.021	0.765	0.007
	7	0.492	0.006	0.545	0.001
80-85	3	0.927	0.098	0.882	0.107
	5	0.794	0.039	0.761	0.012
	7	0.463	0.019	0.455	0.001

Table 4: Efficiencies *vs* N_{Cl}. $\delta_{phot} = 0.05$. Values from fig. 27.

identification cuts give an efficiency of approximately 90 % for both methods.

8.2 Asymmetry

We showed that the selection of the leptonic sample included the possibility for a hadronic contamination. But, since the contamination is small, it only accounts for a difference in efficiencies of $\sim 1\,\%$.

Figure 28 shows the eTRD efficiency when the contamination decreases. On top we show the efficiency for leptons selected with $\chi^2_{pht} < 20$ and on the bottom with $\chi^2_{pht} < 2$ (cleaner sample). First we see that the efficiencies are more constant (less dependent on momentum). In addition, the difference decreases from $\sim 4\,\%$ to $\sim 2\,\%$ in the cleaner sample. This decrease is not real, as we

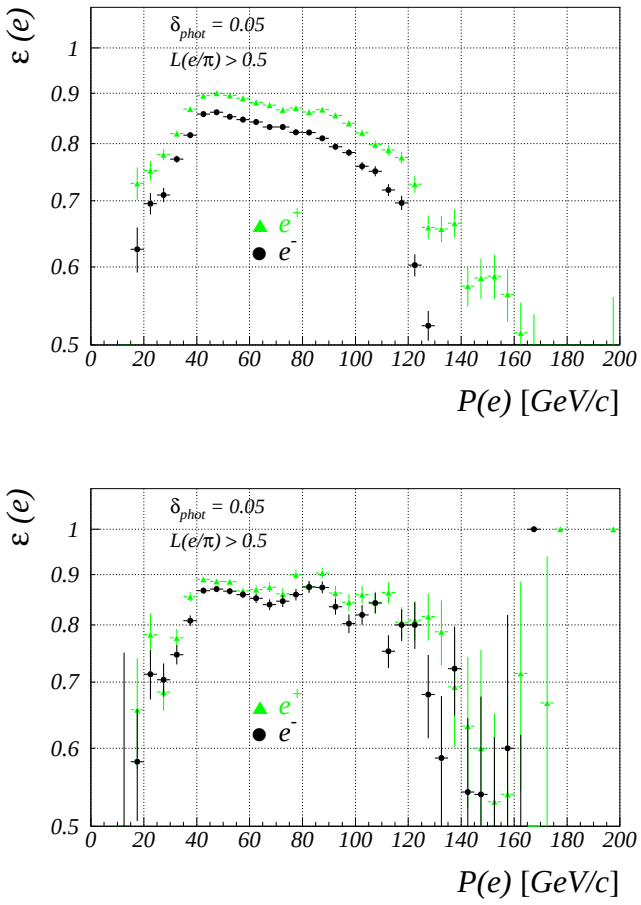

Figure 28: eTRD efficiency, likelihood method. Top: $\chi^2_{pht} < 20$; bottom: $\chi^2_{pht} < 2$.

have mentioned before, it is due to the better efficiencies and, as the main effect, to the inverted efficiencies in group *pp* (see figure 29, bottom); The top figure shows the efficiencies for all groups with exception of *pp*, and we obtain a difference of 4 %. Incorporating also group *pp* the difference decrease to 2 % as shown in figure 28(bottom).

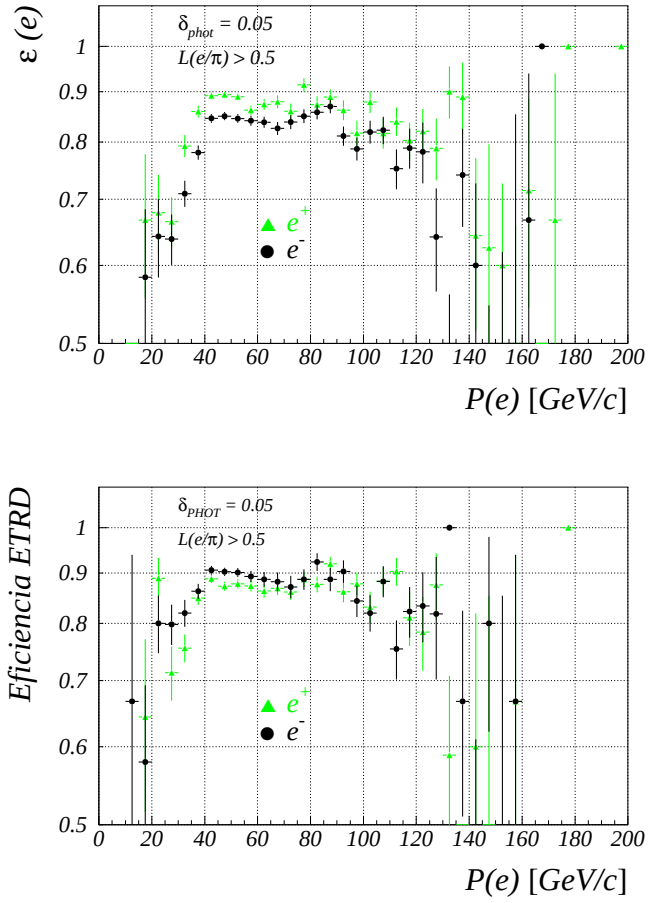

Figure 29: eTRD efficiency, $\chi^2_{pht} < 2$. Likelihood method. Top: groups *pb, px, py, pz*; bottom: group *pp*.

8.3 E/p Distributions en PHOT2

As a result of the selection process for the leptonic sample we found as a side result that the E/p distributions for e^+/e^- is not centered in 1.0. The positron

sample is centered in 0.95 (figure 22), and the electron sample in 0.97 (figure 23). We assign this to a calibration effect in the lead-glass calorimeter.

9 Conclusions

Separating positrons (electrons) with the likelihood method we require that the lepton hypothesis is more likely than the pion hypothesis, or $\mathcal{L}(e/\pi) > 0$. Correlated with the identification efficiency for identifying e^+/e^- the the pion rejection. For our main interest, the semi-leptonic decay of the Λ_c^+, and due to a pre-defined cut in pass1 and pass2 (*strip490*) we conclude that the best compromise between the identification efficiency and the pion rejection is obtain with

$$\mathcal{L}(e/\pi) > 0.5.$$

For the cluster-counting method it is

$$N_{Cl} > 3.$$

The eTRD identification efficiency for positrons (electrons) in approximately constant as a function of momentum, $\epsilon(e) \sim 90\%$.

The likelihood method is more adequate to use than the cluster counting, because it has a higher rejection of pions, of $\sim 99\,\%$, while cluster-counting only provides $\sim 90\,\%$.

We also showed that the observed asymmetry is due to ageing of the detector.

For our analysis, we decided to use the results from fig. 25(top) for positrons, which we summarized in table 5. We apply this momentum-dependent efficiencies as weights.

$p\,[\mathrm{GeV}/c]$	2.5	7.5	12.5	17.5	22.5	27.5	32.5	37.5
$\varepsilon(e^+)$	–	–	0.250	0.656	0.782	0.684	0.776	0.854
$p\,[\mathrm{GeV}/c]$	42.5	47.5	52.5	57.5	62.5	67.5	72.5	77.5
$\varepsilon(e^+)$	0.890	0.886	0.885	0.866	0.869	0.874	0.860	0.900
$p\,[\mathrm{GeV}/c]$	82.5	87.5	92.5	97.5	102.5	107.5	112.5	117.5
$\varepsilon(e^+)$	0.875	0.903	0.862	0.843	0.859	0.843	0.863	0.805

Table 5: Final efficiency values for the eTRD identifying positrons. $\mathcal{L}(e/\pi) > 0.5$, in $5\,\mathrm{GeV}/c$ bins.

A $\mathcal{L}(e/\pi)$ Distributions in the eTRD

The criterion for the identification of the positron (electron) is based on the logarithm of the ration of the likelihoods for the electron and pion hypothesis, $\mathcal{L}(e) > \mathcal{L}(\pi)$. We use $\mathcal{L}(e/\pi) > 0$.

For the lepton sample defined with PHOT2, ($id\_adcgam = 2$, see fig. 8) we have shown that the amount of hadronic contamination depends on the cut δ_{phot}. Figure 30 shows the $\mathcal{L}(e/\pi)$ distributions for $\delta_{phot} = 0.25, 0.15, 0.10, 0.05$. We can see that the majority of the lepton events are in the region $\mathcal{L}(e/\pi) > 0$. The number of entries with $\mathcal{L}(e/\pi) < 0$ decrease as we define a cleaner sample ($\delta_{phot} \to 0$).

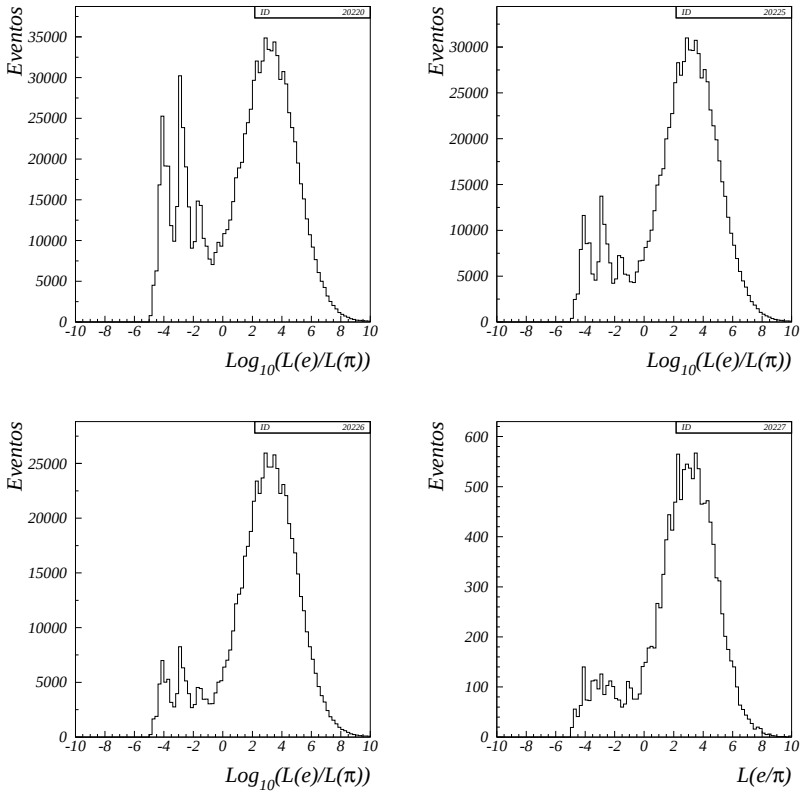

Figure 30: $\mathcal{L}(e/\pi)$ of the eTRD for leptons identified with PHOT2. $id\_adcgam = 2$ with $\delta_{phot} = 0.25$ (top left), $\delta_{phot} = 0.15$ (top right), $\delta_{phot} = 0.10$ (bottom left), $\delta_{phot} = 0.05$ (bottom right).

B N_{Cl} Distributions in the eTRD

Positrons (electrons) emit more transition radiation photon than pions, for this reason a cut in N_{Cl} is a possible criterion for the separation of electron and pions.

Figure 31 shows the number of detected clusters for different hadronic contamination levels, $id\_adcgam = 2$ with $\delta_{phot} = 0.25, 0.15, 0.10, 0.05$ (see fig. 8). As the leptonic sample becomes cleaner ($\delta_{phot} \to 0$), the number of entries in the hadronic region ($N_{Cl} < 3$) decrease, and the leptons stay in $N_{Cl} > 3$.

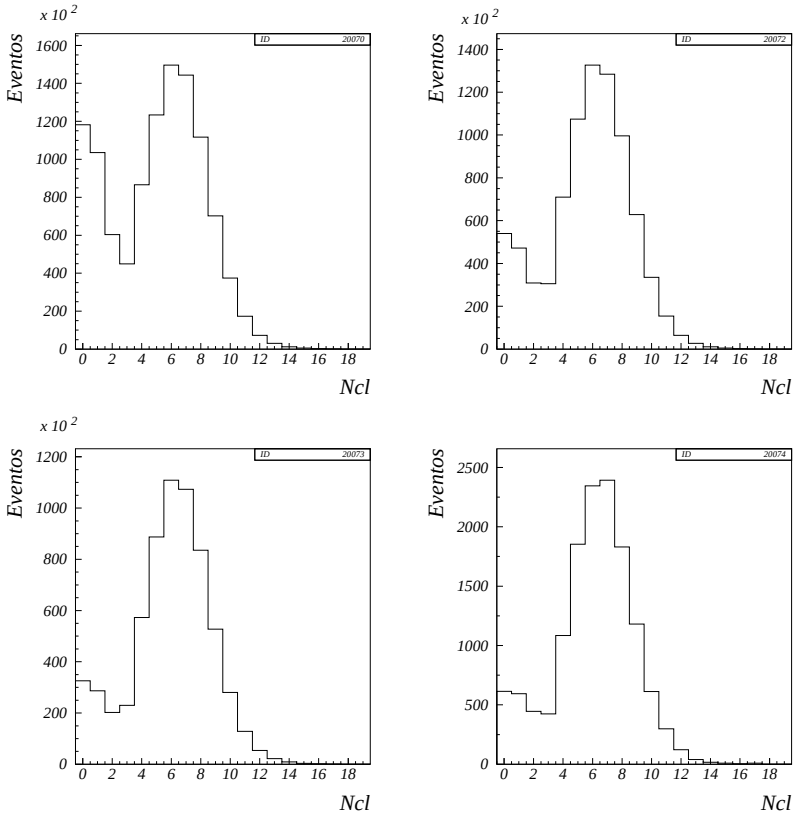

Figure 31: Number of clusters in the eTRD for leptons identified with PHOT2. $id\_adcgam = 2$ with $\delta_{phot} = 0.25$ (top left), $\delta_{phot} = 0.15$ (top right), $\delta_{phot} = 0.10$ (bottom left), $\delta_{phot} = 0.05$ (bottom right).

C Efficiency of the eTRD for different $\mathcal{L}(e/\pi)$

The efficiency depends strongly in the criterion applied to identify positrons (electrons). Here we analyze the eTRD efficiency for different cuts in $\mathcal{L}(e/\pi)$ and δ_{phot}. Specifically, The cuts we used are:

$$\mathcal{L}(e/\pi) > 0.5, 1.5, 2.5$$

and for the E/p window for the definition of the leptonic sample:

$$\delta_{phot} = 0.05, 0.10, 0.15, 0.25$$

First lets look at fig. 32. As we make a harder cut in $\mathcal{L}(e/\pi)$ the eTRD efficiency decreases, for example in the region from $45\,\mathrm{GeV}/c$ to $55\,\mathrm{GeV}/c$: with $\mathcal{L}(e/\pi) > 0.5$ (top plot) we obtain $\sim 87\,\%$; for $\mathcal{L}(e/\pi) > 1.5$ (center plot) $\sim 80\,\%$; $\mathcal{L}(e/\pi) > 2.5$ (lower plot) $70\,\%$. The number of leptons passing the cut is decreasing, like in figure 11.

Two main comments concerning the plots in fig. 32. First we observe that the efficiency decreases for momenta $> 45\,\mathrm{GeV}/c$ and decreases even more abruptly for higher momenta $\sim 120\,\mathrm{GeV}/c$. This is due to the hadronic contamination of the lepton sample, which increases with increasing momenta, leading to an apparent decrease in efficiency. We prove this argument in appendix H, where we show the efficiency as a function of χ^2_{pht}.

The second observation is related to the noticeable difference the positron and electron efficiency. As mentioned before, this asymmetry should not exist. We believe that it has at least something to do with the hadronic contamination, or with ageing of part of the detector. To check the effect of the hadronic contamination, we refer to fig. 33. As δ_{phot} increases, the efficiency decreases. At higher values of δ_{phot} we have a larger contamination (see fig. 8), leading again to an apparent decrease in efficiency.

The contamination is larger in the electron sample than in the positron sample, as seen in figures 22 and 23. Figure 34 shows the difference in efficiencies, and we see that as δ_{phot} increases the difference increases as well.

C.1 Efficiency for positron (electron), $\delta_{phot} = 0.05$

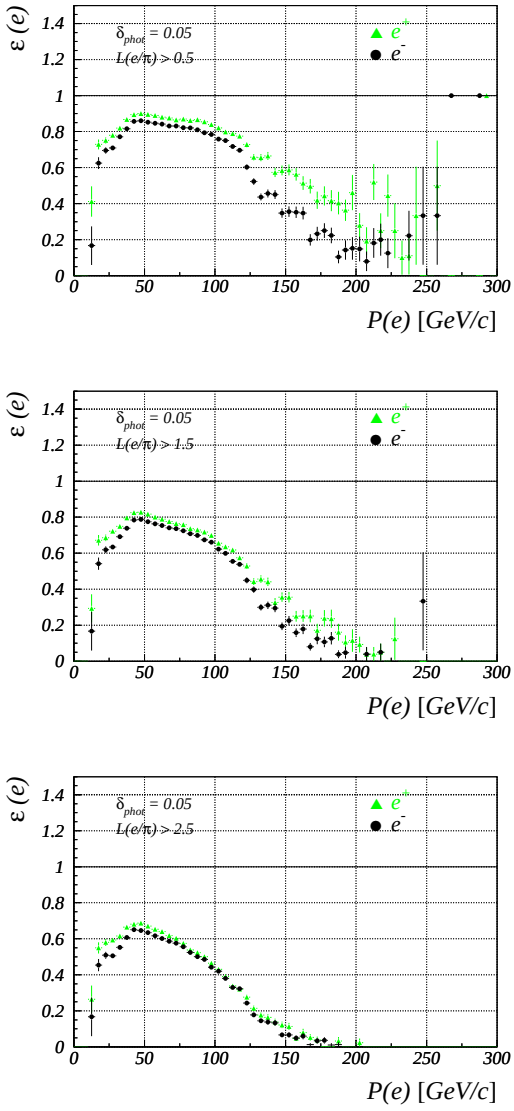

Figure 32: eTRD efficiencies for positron and electron, for different cuts in likelihood ratio. Top: $\mathcal{L}(e/\pi) > 0.5$; center: $\mathcal{L}(e/\pi) > 1.5$; bottom: $\mathcal{L}(e/\pi) > 2.5$.

C.2 eTRD efficiency as function of δ_{phot}

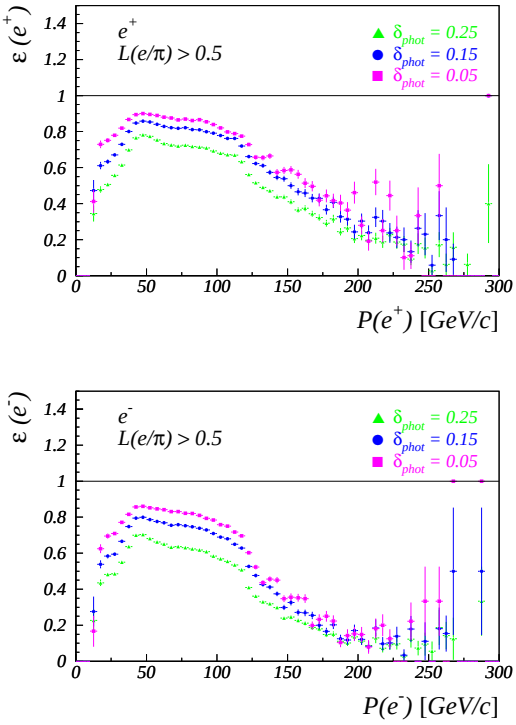

Figure 33: eTRD efficiency for positrons (top) and electrons (bottom) for different values of δ_{phot}, with $\mathcal{L}(e/\pi) > 0.5$.

C.3 Differences in the eTRD efficiencies as function of δ_{phot}

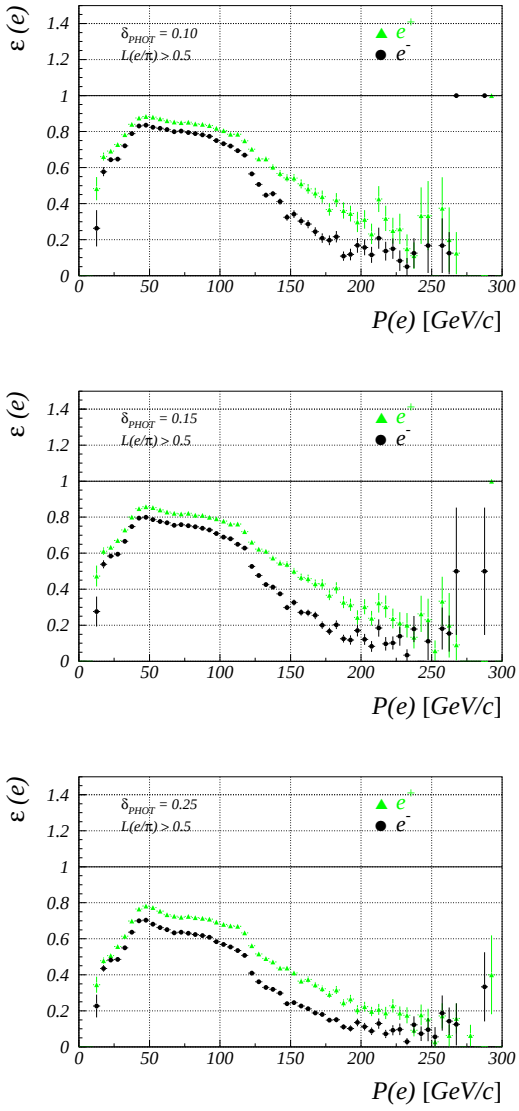

Figure 34: eTRD efficiencies for the identification of positrons (electrons) for different values of δ_{phot}, with $\mathcal{L}(e/\pi) > 0.5$. Top: $\delta_{phot} = 0.10$; center: $\delta_{phot} = 0.15$; bottom: $\delta_{phot} = 0.25$.

D eTRD Efficiency, N_{Cl}

We obtained the eTRD efficiency for the positron (electron) identification for different values of δ_{phot} and N_{Cl}. We observe a similar behavior of the efficiencies as with the likelihood method.

The cuts we used for the identification criteria are:

$$\mathcal{N}_{Cl} > 3, 5, 7;$$

and for the definition of the leptonic sample in PHOT2:

$$\delta_{phot} = 0.05, 0.10, 0.15, 0.25.$$

As we apply a harder cut in N_{Cl}, fewer particles pass the cut, (see fig. 12), leading to a decrease in identification efficiency. We measured the efficiency for values of $N_{Cl} > 3, 5, 7$, for a fixed value of δ_{phot}, fig. 35. As we apply a harder cut in N_{Cl} the eTRD efficiency decreases. For example, from $45 - 55\,\mathrm{GeV}/c$, we observe a decrease from $\sim 90\,\%$ ($N_{Cl} > 3$, top) over $80\,\%$ ($N_{Cl} > 5$, center) to $50\,\%$ ($N_{Cl} > 7$, bottom)

As the value of δ_{phot} decreases, the eTRD efficiency increases, due to the decrease in hadronic contamination, see fig. 36.

The difference in efficiency is at least partly caused by the contamination, as seen in figures 22 and 23. Figure 37 shows the difference in efficiencies, as δ_{phot} increases (higher contamination) the difference increases as well.

D.1 Number of Cluster, $\delta_{phot} = 0.05$

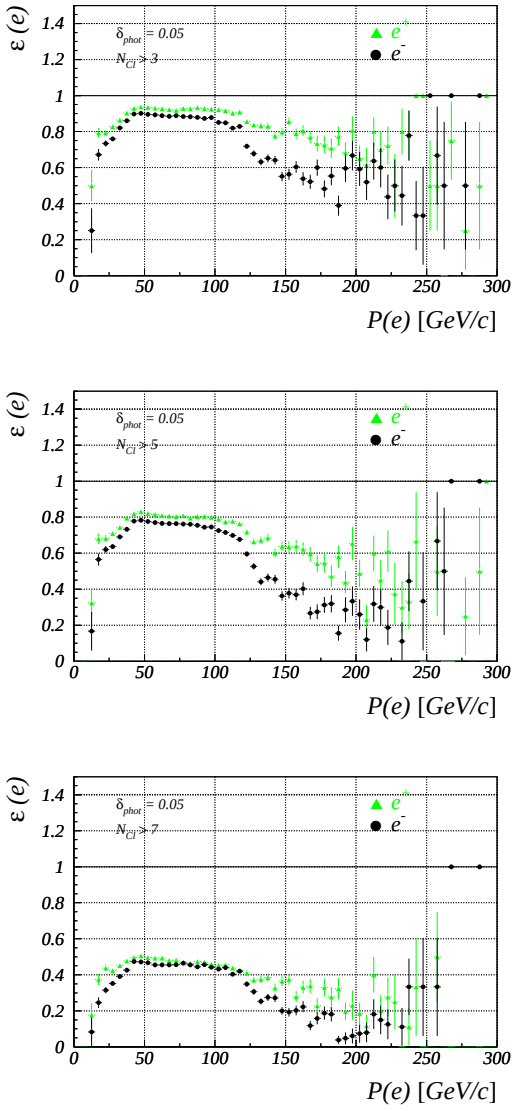

Figure 35: eTRD efficiencies of positrons and electrons, for different cuts: Top: $N_{Cl} > 3$; center: $N_{Cl} > 5$; bottom $N_{Cl} > 7$.

D.2 eTRD efficiency, Number of Cluster, $\delta_{phot} = 0.25, 0.15, 0.10$

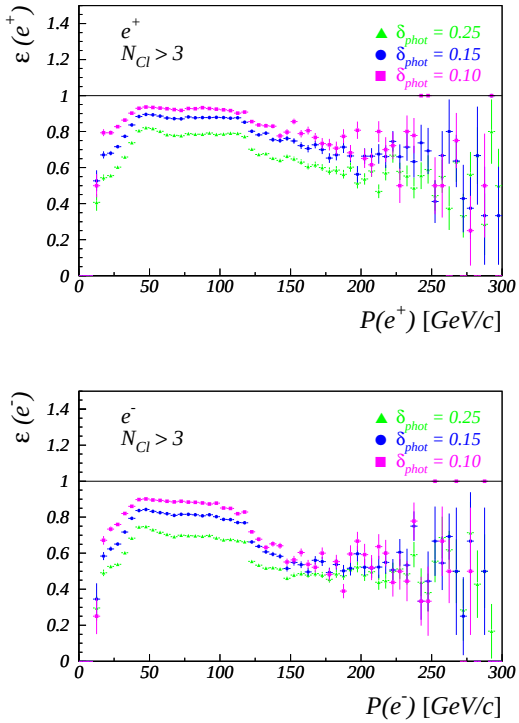

Figure 36: eTRD efficiency for different values of δ_{phot}, for positrons (top) and electrons (bottom). $N_{Cl} > 3$.

D.3 Differences in efficiency, Number of clusters, as function of δ_{phot}

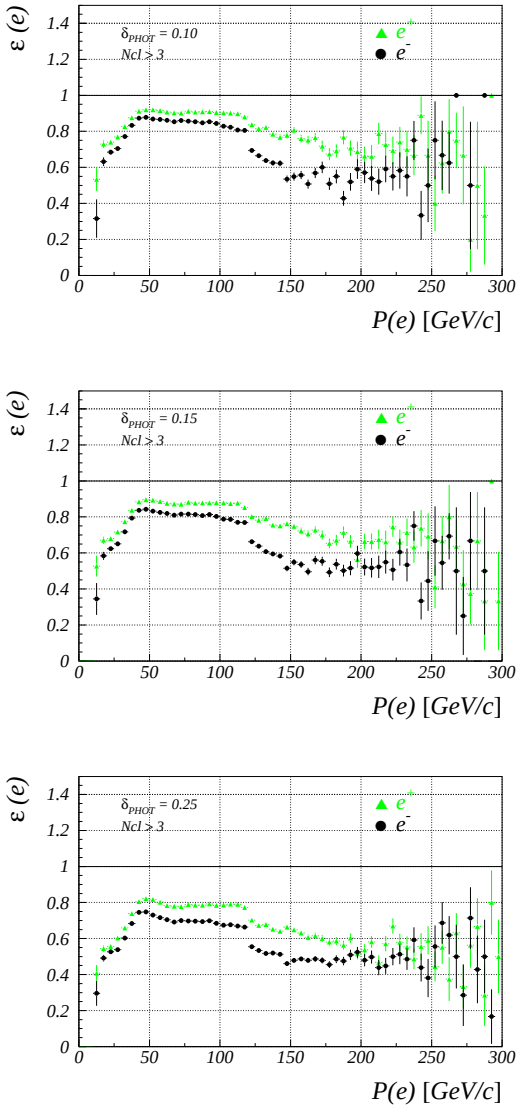

Figure 37: eTRD efficiencies for positrons and electrons, for different cuts in the selection of the leptonic sample: Top: $\delta_{phot} = 0.10$; center: $\delta_{phot} = 0.15$; bottom: $\delta_{phot} = 0.25$. $N_{Cl} > 3$.

E Pion Miss-Identification

E.1 Pion Miss-Identification – $\mathcal{L}(e/\pi)$

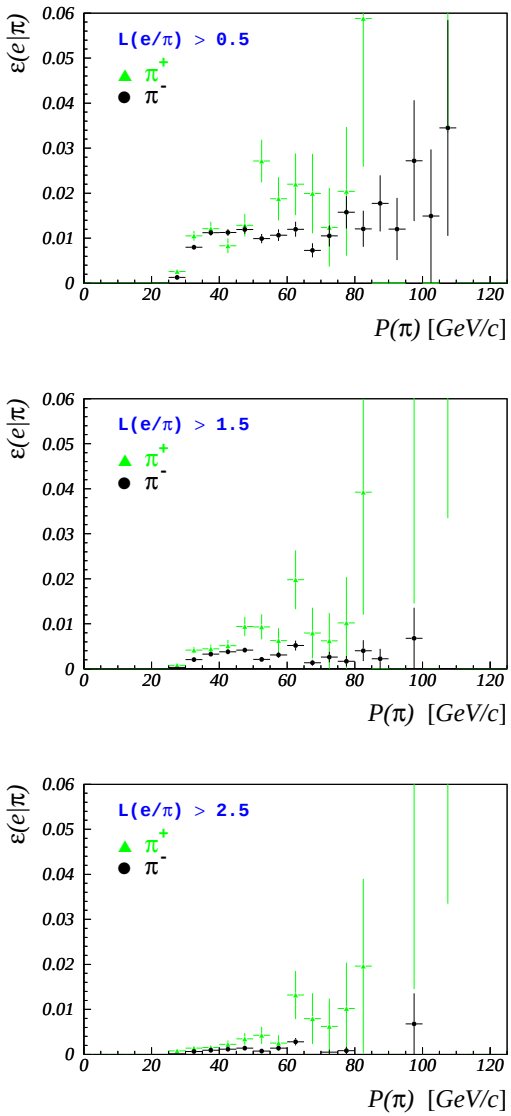

Figure 38: Pion Miss-identification for different cuts in $\mathcal{L}(e/\pi)$: Top: $\mathcal{L}(e/\pi) > 0.5$; center: $\mathcal{L}(e/\pi) > 1.5$; bottom: $\mathcal{L}(e/\pi) > 2.5$.

E.2 Pion Miss-Identification – N_{Cl}

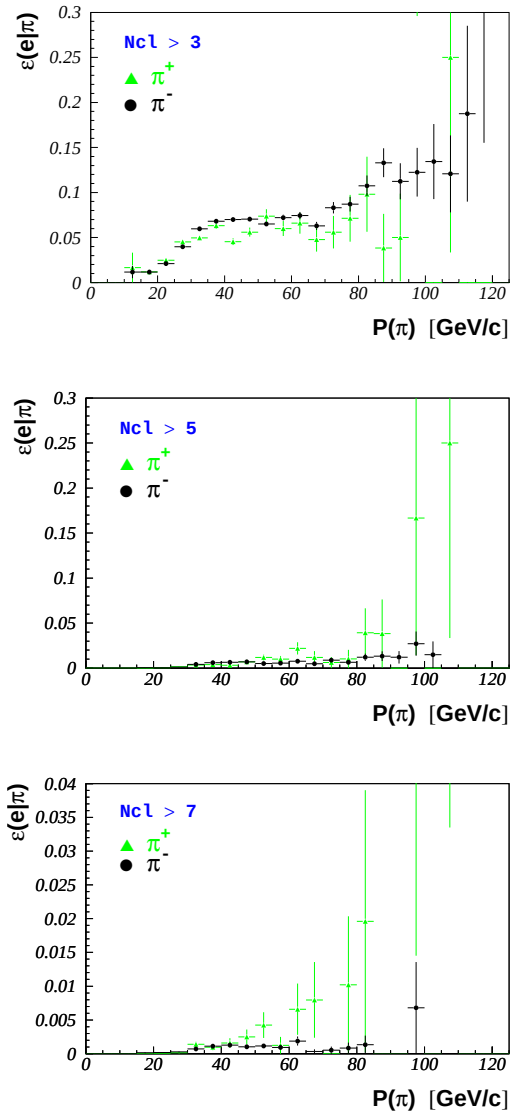

Figure 39: Pion Miss-identification for different cuts in N_{Cl}: Top: $N_{Cl} > 3$; center: $N_{Cl} > 5$; bottom: $N_{Cl} > 7$.

F Efficiency for different run groups

With the goal to determine the behavior of the eTRD as a function of time, we measured the efficiencies $\epsilon(e^{\pm})$ for each run group. Figures 40 and 41 show the results.

In groups *pb, pc* and *pd* both efficiencies are similar, and groups *pe, pf, pg, ph, px, py,* and *pz* show differences in the efficiencies, with $\epsilon(e^-) < \epsilon(e^+)$. Opposite to the other groups, *pp* shows a inversion of the efficiencies, now $\epsilon(e^-) > \epsilon(e^+)$ (which is for positive beam, the particles are bend the other way).

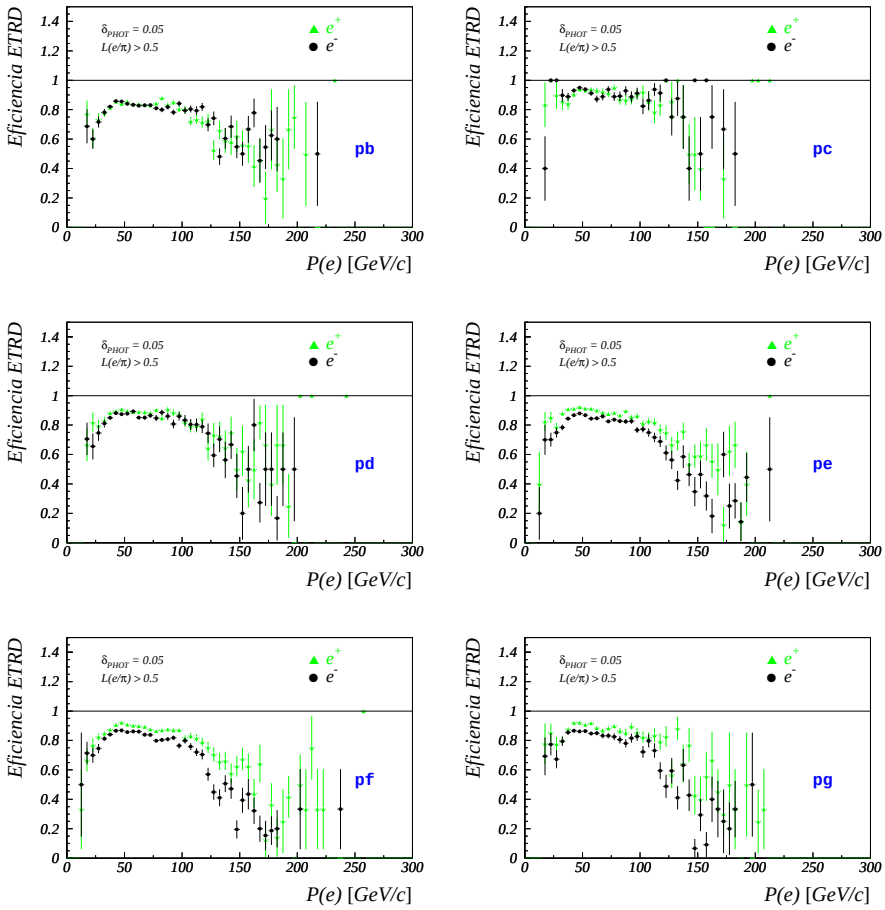

Figure 40: eTRD efficiencies for the identification of positrons (green) and electrons (black) for different run groups. $\delta_{phot} = 0.05$, $\mathcal{L}(e/\pi) > 0.5$.

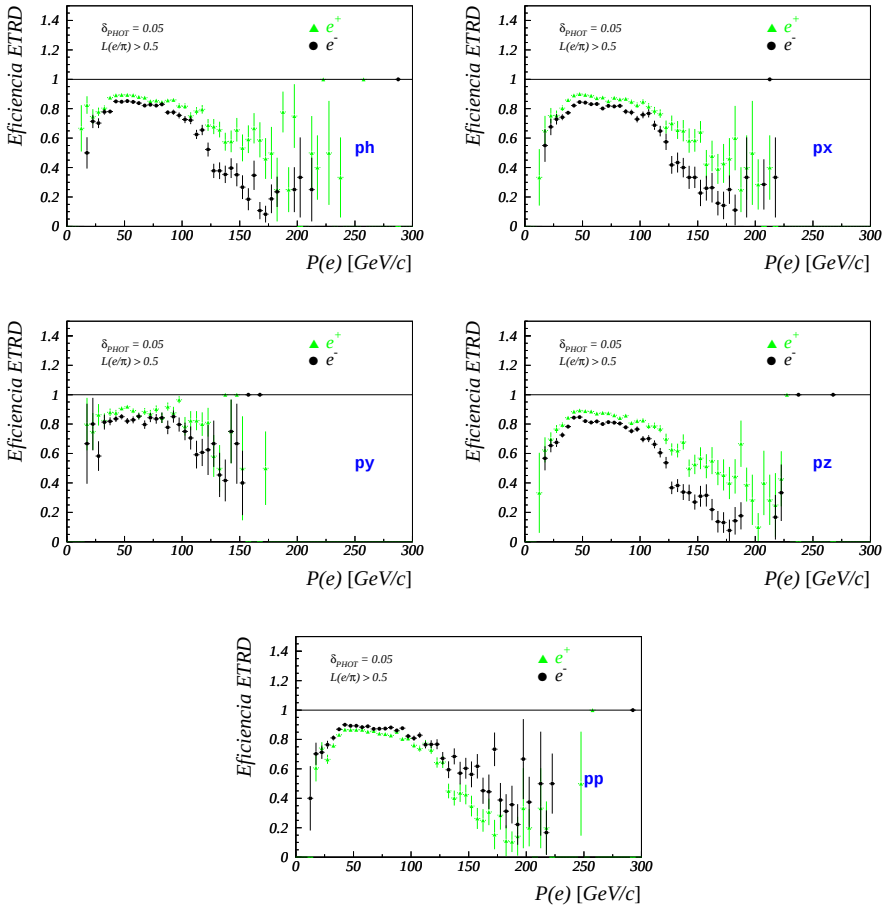

Figure 41: eTRD efficiencies for the identification of positrons (green) and electrons (black) for different run groups. $\delta_{phot} = 0.05$, $\mathcal{L}(e/\pi) > 0.5$.

G Asymmetry for different run groups

The asymmetry of the efficiencies for each run group are shown in figures 42 and 43. As a reminder the asymmetry is defined as $\mathcal{A} = \epsilon(e^+)/\epsilon(e^-)$.

The groups *pb, pc* and *pd* do not present any asymmetry, $\mathcal{A} = 1$. Groups *pe, pf, pg, ph, px, py,* and *pz* present $\mathcal{A} > 1$, $\epsilon(e^+) > \epsilon(e^-)$. As opposed to the previous groups, *pp* presents an asymmetry $\mathcal{A} < 1$, $\epsilon(e^+) < \epsilon(e^-)$; the positive data were taken towards the end of the experiment.

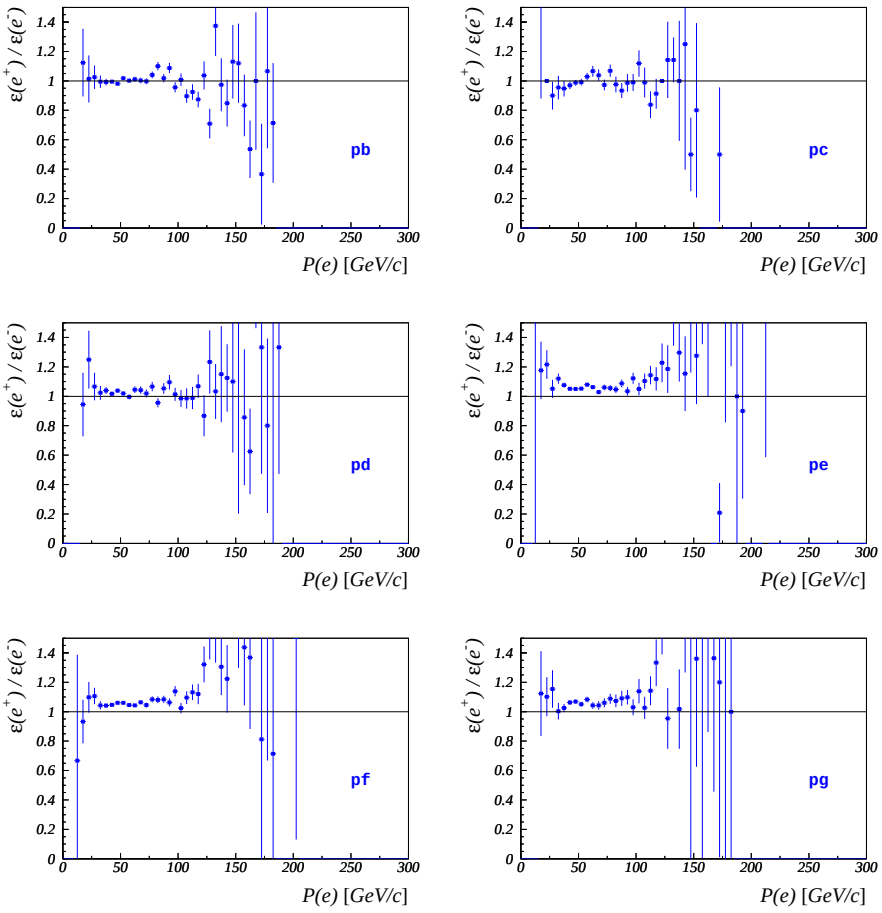

Figure 42: Asymmetry of the efficiencies for different run groups. $\delta_{phot} = 0.05$, $\mathcal{L}(e/\pi) > 0.5$.

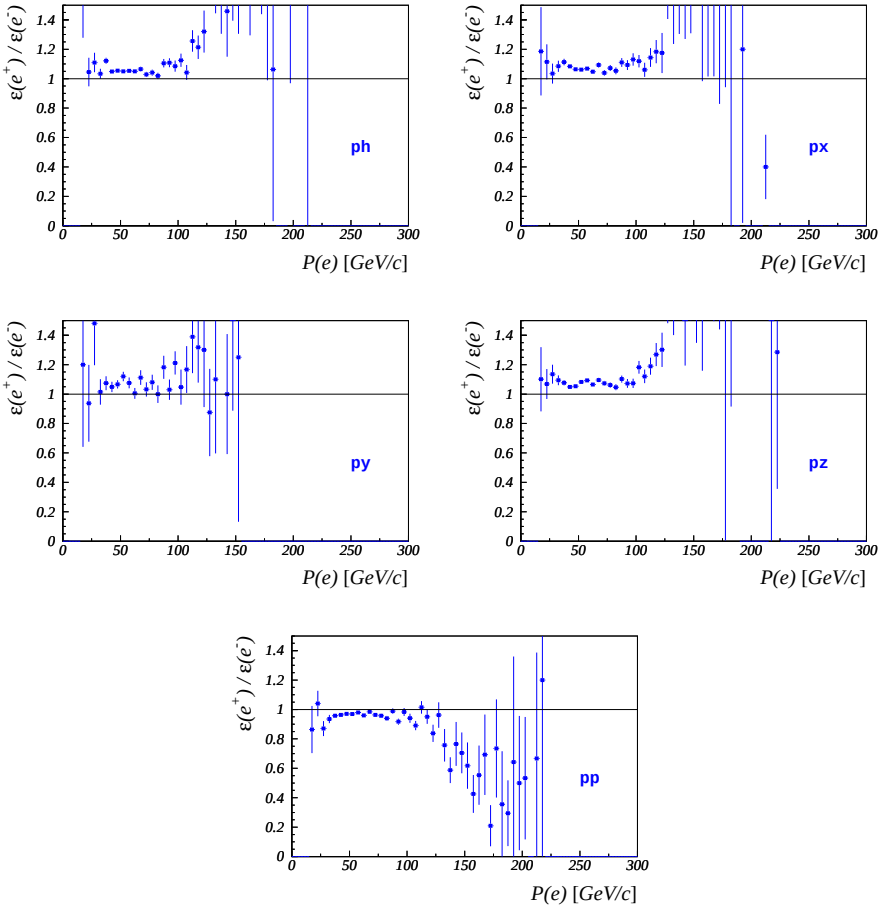

Figure 43: Asymmetry of the efficiencies for different run groups. $\delta_{phot} = 0.05$, $\mathcal{L}(e/\pi) > 0.5$.

H Efficiency as a function of χ^2_{pht}

With the goal of selecting a leptonic sample free of any hadronic combination we applied a harder cut in χ^2_{pht} in the cluster-shape algorithm of the calorimeter software.

Figure 44 show the efficiencies for different values of χ^2_{pht}. The standard code for the identification of positrons in the calorimeter has a default cut of $\chi^2_{pht} < 20$.

Applying a harder cut in χ^2_{pht} results in that the efficiency for identifying electrons moves towards the values for positrons; in addition, the efficiency for momenta above $120\,\mathrm{GeV}/c$ increases to such an extend that we call it constant, independent of the momentum.

Finally, we studied the efficiencies and the asymmetry with a cut at $\chi^2_{pht} < 2$. Figures 45, 46 and 47 show the results.

The efficiencies for each run groups are shown in figure 45. We observe that the difference in efficiencies stays the same, and group *pp* shows again an inversion of the efficiencies with respect to the other groups.

Figure 46(center) still shows a clear difference in the efficiencies for momenta $50-80\,\mathrm{GeV}/c$, demonstrating that the asymmetry is not caused by the hadronic contamination. The inversion in group *pp* is additional evidence that the ageing of part of the detector is the reason the observed asymmetry.

Figure 46(bottom) shows the efficiency of the eTRD for the identification of positron and electrons. The difference is small, but again this is due to the inclusion of group *pp* into this average.

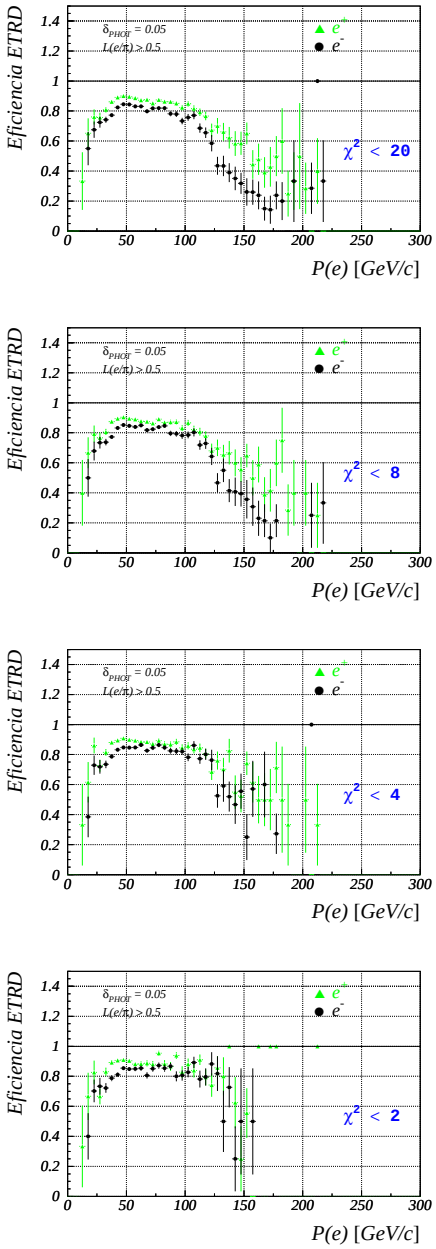

Figure 44: eTRD efficiencies for different χ^2_{pht}. Top: $\chi^2_{pht} < 20$; center-top: $\chi^2_{pht} < 8$; center-bottom: $\chi^2_{pht} < 4$; bottom: $\chi^2_{pht} < 2$.

H.1 Efficiencies for different run groups, $\chi^2_{pht} < 2$

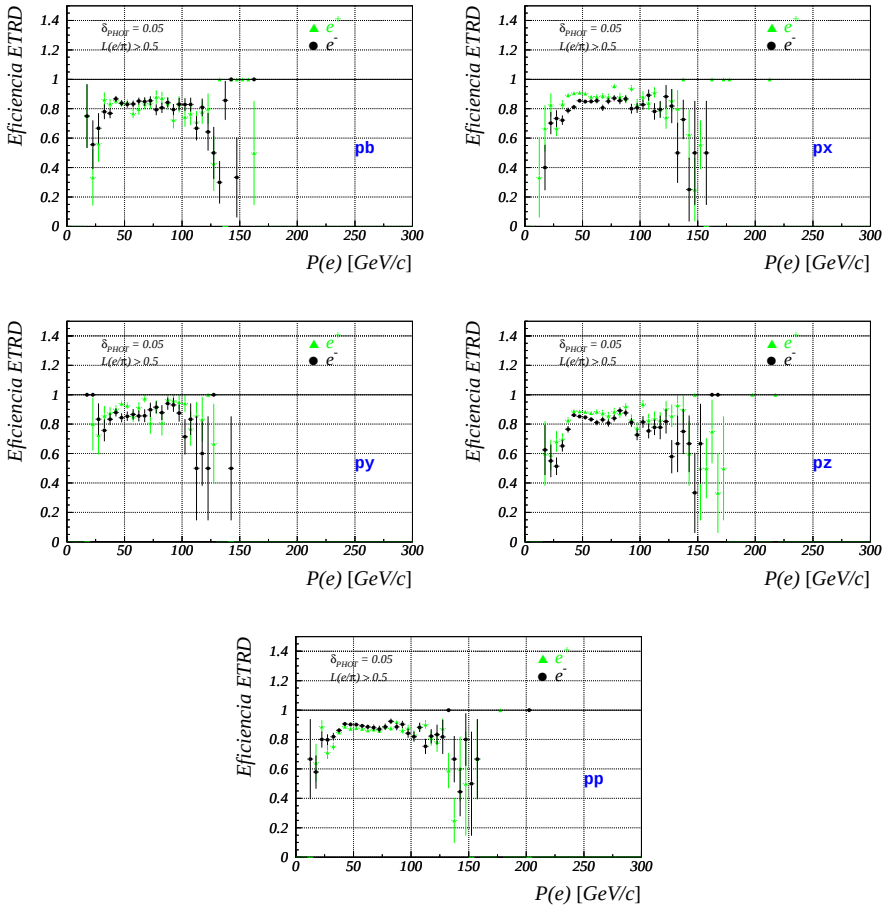

Figure 45: eTRD efficiencies for the identification of positrons (green) and electrons (black) for different run groups. $\delta_{phot} = 0.05$, $\mathcal{L}(e/\pi) > 0.5$.

H.2 Efficiency as a function of time, $\chi^2_{pht} < 2$

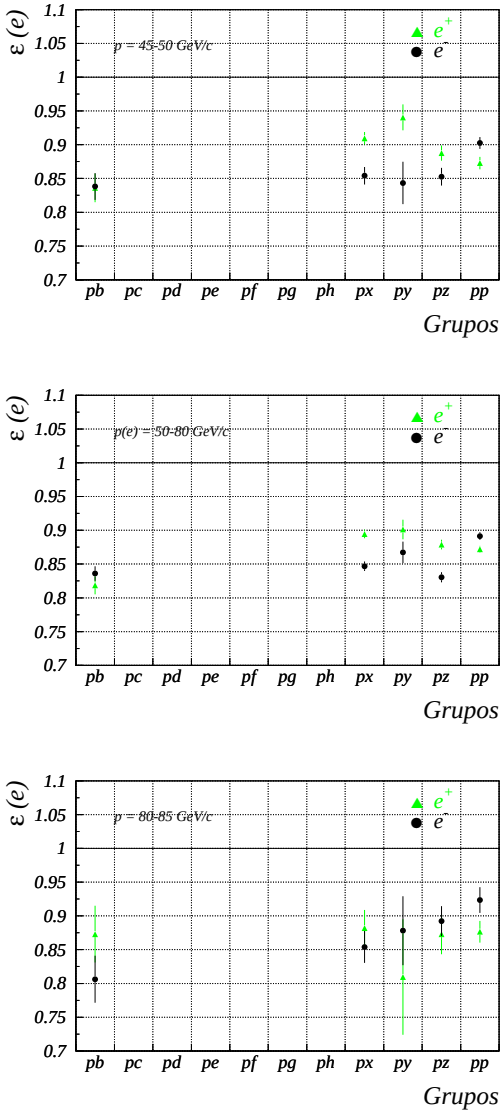

Figure 46: eTRD efficiencies for the identification of positrons (green) and electrons (black) for different run groups. $\delta_{phot} = 0.05$, $\mathcal{L}(e/\pi) > 0.5$, $\delta r = 0.7\,cm$.

H.3 Average eTRD efficiencies, $\chi^2_{pht} < 2$

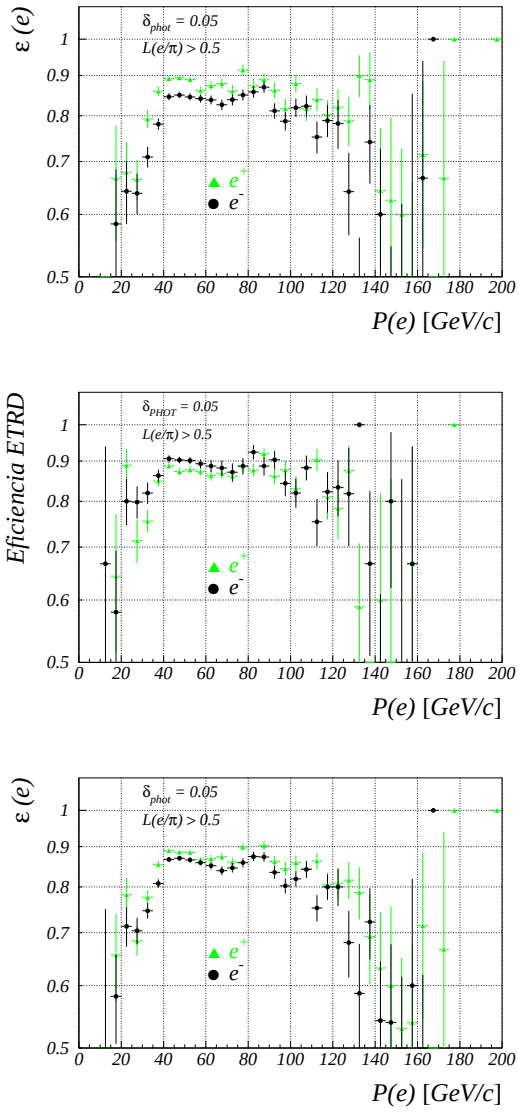

Figure 47: eTRD efficiencies, $\chi^2_{pht} < 2$. Likelihood method. Top: groups *pb, px, py, pz*; center: group *pp*; bottom: groups *pb, px, py, pz* and *pp*.

I eTRD efficiency as a function of the number of segments

We analyzed the 1M run to see of the efficiency depends on the number of segments within the acceptance of the eTRD.

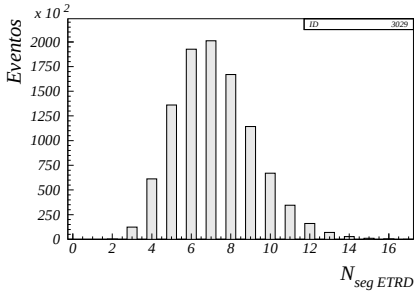

Figure 48: Multiplicity of the segments in the eTRD.

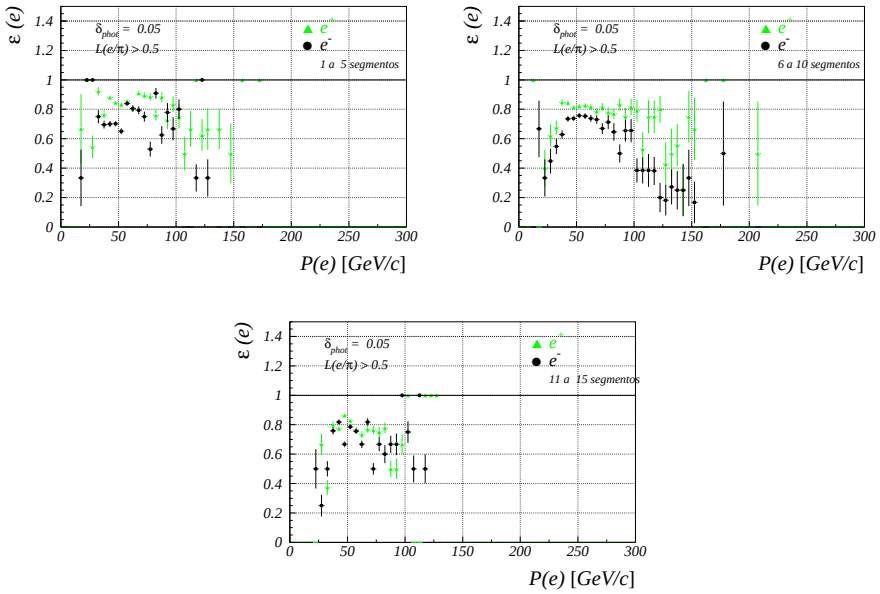

Figure 49: Efficiency for different number segments in the eTRD.

References

[1] Jorge Amaro Reyes, Jurgen Engelfried, $\Lambda_c^+ \to \Lambda(1520)e^+\nu$ branching fraction. H-Note 879, SELEX Internal note, January 2006.

[2] V. Maleev et al., *Description an test results for DPWC and TRD in E781*, H-Note 747, SELEX Internal Note, 1995

[3] M.K.A. Antonov, G. Dsyubenko, *Geometry of the assembled E781 Photon 1,2 detectors*, H-Note 748, SELEX Internal Note, 1995.

[4] V.V.G. Davidenko, M. Kubanntsev, *Photon database for E781*, H-Note 767, SELEX Internal Note, 1996.

[5] M.Y. Balatz et al., *The lead-glass electromagnetic calorimeter for the SELEX experiment*, H-Note 845, SELEX Internal Note, 2004.

[6] N. Terentyev, *Particle Identification in E781 with eTRD and BTRD*, E781 Offline Workshop, 1997.

[7] Nikolai Kuropatkin, *Generalized Likelihood Method for Lepton Identification in SELEX*, H-Note 806, SELEX Internal Note, 1998.

[8] Particle Data Group, C. Caso *et al.*, Eur. Phys. J. **C3**, 1 (1998).